



# Neuronal Constituents and Putative Interactions Within the *Drosophila* Ellipsoid Body Neuropil

Jaison Jiro Omoto<sup>1,2†</sup>, Bao-Chau Minh Nguyen<sup>1†</sup>, Pratyush Kandimalla<sup>1</sup>, Jennifer Kelly Lovick<sup>1</sup>, Jeffrey Michael Donlea<sup>2</sup> and Volker Hartenstein<sup>1\*</sup>

<sup>1</sup> Department of Molecular, Cell, and Developmental Biology, University of California, Los Angeles, Los Angeles, CA, United States, <sup>2</sup> Department of Neurobiology, University of California, Los Angeles, Los Angeles, CA, United States

## OPEN ACCESS

### Edited by:

Claude Desplan,  
New York University, United States

### Reviewed by:

Makoto Sato,  
Kanazawa University, Japan  
Giorgio F. Gilestro,  
Imperial College London,  
United Kingdom

### \*Correspondence:

Volker Hartenstein  
volkerh@mcdob.ucla.edu

<sup>†</sup>These authors have contributed  
equally to this work

**Received:** 02 August 2018

**Accepted:** 26 October 2018

**Published:** 27 November 2018

### Citation:

Omoto JJ, Nguyen B-CM, Kandimalla P, Lovick JK, Donlea JM and Hartenstein V (2018) Neuronal Constituents and Putative Interactions Within the *Drosophila* Ellipsoid Body Neuropil.  
*Front. Neural Circuits* 12:103.  
doi: 10.3389/fncir.2018.00103

The central complex (CX) is a midline-situated collection of neuropil compartments in the arthropod central brain, implicated in higher-order processes such as goal-directed navigation. Here, we provide a systematic genetic-neuroanatomical analysis of the ellipsoid body (EB), a compartment which represents a major afferent portal of the *Drosophila* CX. The neuropil volume of the EB, along with its prominent input compartment, called the bulb, is subdivided into precisely tessellated domains, distinguishable based on intensity of the global marker DN-cadherin. EB tangential elements (so-called ring neurons), most of which are derived from the DALv2 neuroblast lineage, predominantly interconnect the bulb and EB domains in a topographically organized fashion. Using the DN-cadherin domains as a framework, we first characterized this connectivity by Gal4 driver lines expressed in different DALv2 ring neuron (R-neuron) subclasses. We identified 11 subclasses, 6 of which correspond to previously described projection patterns, and 5 novel patterns. These subclasses both spatially (based on EB innervation pattern) and numerically (cell counts) summate to the total EB volume and R-neuron cell number, suggesting that our compilation of R-neuron subclasses approaches completion. EB columnar elements, as well as non-DALv2 derived extrinsic ring neurons (ExR-neurons), were also incorporated into this anatomical framework. Finally, we addressed the connectivity between R-neurons and their targets, using the anterograde *trans*-synaptic labeling method, *trans*-Tango. This study demonstrates putative interactions of R-neuron subclasses and reveals general principles of information flow within the EB network. Our work will facilitate the generation and testing of hypotheses regarding circuit interactions within the EB and the rest of the CX.

**Keywords:** *Drosophila*, ellipsoid body, central complex, neuroblast, ring neurons, *trans*-Tango

## INTRODUCTION

The central complex (CX) is an evolutionarily conserved, higher-order neuropil in the arthropod brain thought to integrate sensory and motor information to coordinate and maintain locomotor behavior, thus enabling appropriate navigation. *Drosophila* mutations that produce structural abnormalities in CX neuropils result in flies with deficiencies in walking and flight

(Strauss and Heisenberg, 1993; Martin et al., 1999). More targeted manipulations, such as silencing of specific CX neuron subclasses, compromise vision-based memories associated with spatial orientation and location (Neuser et al., 2008; Ofstad et al., 2011). Similar themes emerge from anatomical, electrophysiological, and behavioral studies investigating the CX in other insects. In the cockroach CX, for example, single unit activity correlated with changes in locomotor intensity, turning behavior, or heading direction have been identified (Bender et al., 2010; Guo and Ritzmann, 2013; Varga and Ritzmann, 2016). In addition, electrical stimulation of CX neurons in the freely walking cockroach has yielded direct evidence linking CX activity to downstream locomotor output (Martin et al., 2015). In other insects, such as locust, cricket, monarch butterfly, and dung beetle, neurons in the CX are tuned to celestial visual cues such as the sun or pattern of polarized skylight. These cues provide the stable environmental signals required to accurately derive relative heading information for short or long range navigations (Heinze and Homberg, 2007; Heinze and Reppert, 2011; el Jundi et al., 2014, 2015).

The CX consists of four neuropil compartments: the upper (CBU) and lower (CBL) halves of the central body (CB), protocerebral bridge (PB), and paired noduli (NO) (Hanesch et al., 1989; Strausfeld, 2012; Ito et al., 2014). In *Drosophila*, the upper and lower halves of the CB are designated as the fan-shaped body (FB) and ellipsoid body (EB), respectively (Figure 1A). Recently, the asymmetrical body, a paired neuropil located ventral of the FB and adjacent to the NO, has been proposed as a fifth neuropil compartment of the CX (Wolff and Rubin, 2018). These neuropil compartments are largely formed by two orthogonally arranged neuronal populations: (1) columnar (small-field) neurons which interconnect the CX compartments along the antero-posterior axis; (2) tangential (large-field) neurons which provide input from lateral brain neuropils to the CX (Figures 1B,C). Terminal arborizations of these neurons define distinct vertical columns and horizontal layers that can be visualized by markers for synaptic or cell adhesion proteins that globally label, but exhibit variable density in, the neuropil. Based on Bruchpilot immunostaining, seven layers were identified in the *Drosophila* CBU (=FB; Figure 1A) (Wolff et al., 2015). The CBL (=EB) also exhibits a layered organization (Pfeiffer and Homberg, 2014). In *Drosophila*, this compartment undergoes a morphogenetic transformation during pupal development, whereby the lateral ends of the originally bar-shaped EB primordium bend ventrally to adopt a toroidal arrangement (Young and Armstrong, 2010a; Lovick et al., 2017; Xie et al., 2017; Figure 1A). As a result, tangential neurons of the EB display a circular shape, and hence were called “ring neurons” (Hanesch et al., 1989; Figure 1C). Likewise, layers within the EB are annuli, rather than horizontal slabs (Figure 1A). Based on labeling with DN-cadherin, we have defined five distinct annular domains, termed anterior (EBa), inner and outer central (EBic and EBoc), and inner and outer posterior (EBip and EBop) domains (Omoto et al., 2017; Figures 1D–G).

Clonal studies in *Drosophila* show that the neuronal architecture of the CX is organized into lineage-based modules

(Ito and Awasaki, 2008; Yang et al., 2013), a ground plan that is likely conserved across insects (Boyan et al., 2017). A lineage refers to the set of sibling neurons derived from an individual neural progenitor called a neuroblast, and the entire central brain is generated from a fixed number of approximately 100 of such neuroblasts. Four lineages (DM1–4; Figure 1A) give rise to the large number of columnar neurons of the CX (Ito and Awasaki, 2008; Yang et al., 2013). The great diversity observed among these neurons is achieved via temporal patterning of molecular determinants in dividing progenitors (Bayraktar and Doe, 2013; Wang et al., 2014; Doe, 2017). Lineages giving rise to the tangential neurons of the CX have been characterized morphologically (Larsen et al., 2009; Spindler and Hartenstein, 2010; Ito et al., 2013; Wong et al., 2013; Yang et al., 2013; Yu et al., 2013), but have not yet received much attention experimentally. The most notable exception is lineage DALv2/EBa1 (henceforth called DALv2), that generates ring neurons of the EB (Neuser et al., 2008; Seelig and Jayaraman, 2013; Omoto et al., 2017; Figure 1A). Ring neurons project their axons to distinct annular domains of the EB, and typically possess short globular dendrites (“microglomeruli”) in the bulb (BU), a neuropil compartment located laterally adjacent to the EB (Figure 1A). The BU encompasses three main partitions [anterior (BUa), superior (BUs), and inferior (BUi) bulb] that are associated with different annular domains of the EB (Figures 1E–G). Furthermore, the BUs and BUi appear to be divisible into anterior (aBUs/aBUi; Figure 1F) and posterior (pBUs/pBUi; Figure 1G) regions. Input to the BU is provided by neurons of two additional lineages, DALcl1 and DALcl2 (also called AOTUv3 and AOTUv4, respectively) (Wong et al., 2013; Yang et al., 2013; Yu et al., 2013; Omoto et al., 2017). As part of the anterior visual pathway, DALcl1/2 form so-called tubercular-bulbar (TuBu) neurons which project from the anterior optic tubercle to the BU, relaying visual information to ring neurons and thereby the CX as a whole (Omoto et al., 2017; Shiozaki and Kazama, 2017; Sun et al., 2017). TuBu neurons form two lineally segregated parallel channels, with DALcl1 establishing connections with ring neurons located in the peripheral domain of the EB via the BUs, and DALcl2 with central ring neurons via the BUi (Omoto et al., 2017; Shiozaki and Kazama, 2017; Figure 1A).

Detailed functional studies are beginning to shed light on the circuitry involving ring neurons and their TuBu afferents and columnar efferents. Two-photon calcium imaging has revealed a discrete focus of neural activity, or “bump,” within a population of columnar neurons (“E-PGs”) that interconnect the EB, PB, and gall (GA) of the LAL. E-PG neurons encode an internal compass representation via the activity bump, which dynamically tracks the fly’s heading (Seelig and Jayaraman, 2015; Figure 1A). Additional columnar neuron populations that interconnect the PB, EB, and NO, called P-EN neurons, compute the animals’ heading by controlling the movement of the bump in the clockwise or counter-clockwise direction (Green et al., 2017; Turner-Evans et al., 2017). These findings suggest that the EB may operate as a critical hub in the CX, acting as an interface between neurons that transmit and distribute sensory

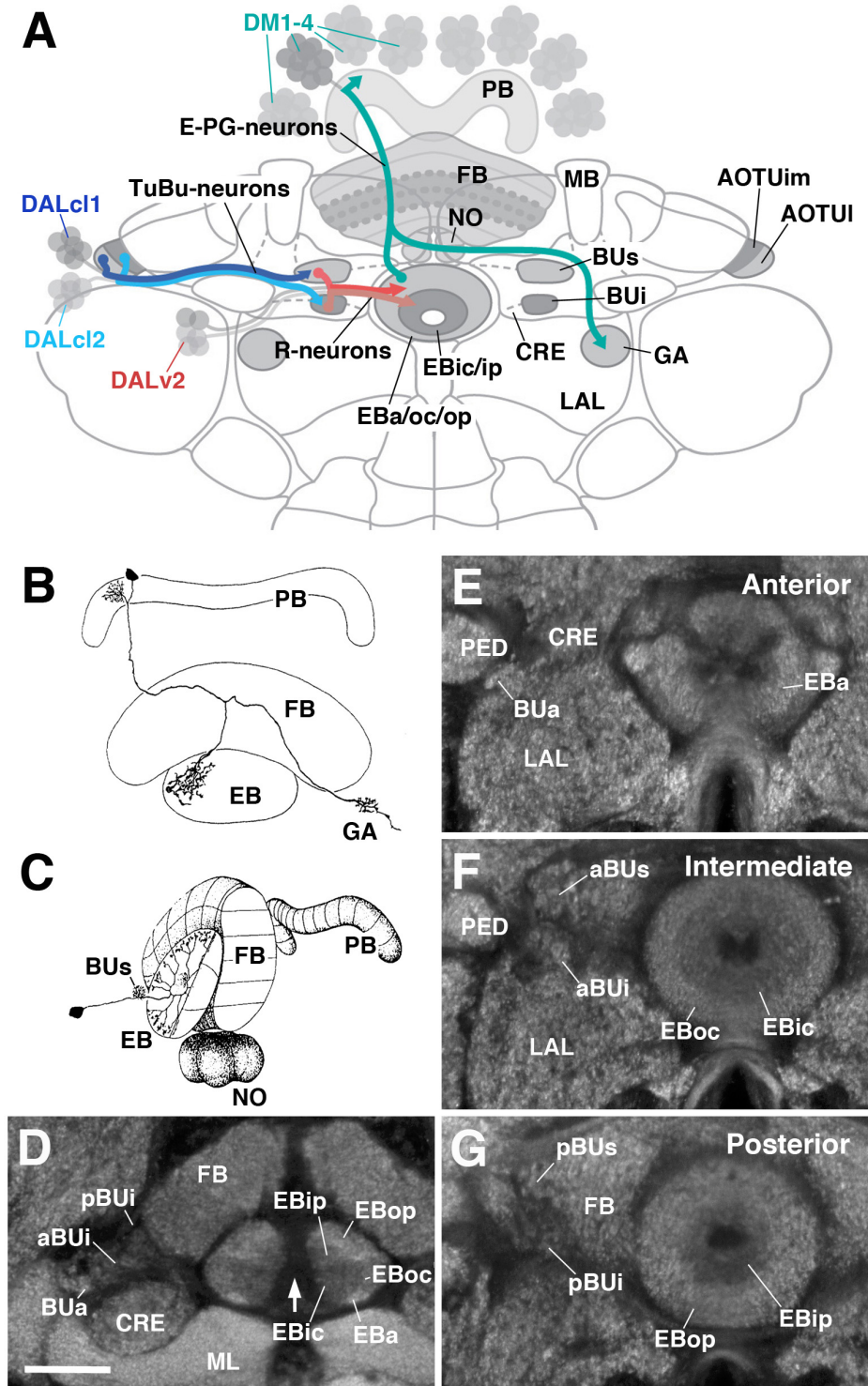


**FIGURE 1 |** General overview of the ellipsoid body (EB): neuronal interactions and compartmentalization. **(A)** Schematized overview of interacting neuronal populations of the EB. Gray indicates relevant lineages, neuron types, and neuropil compartments. The anterior visual pathway, divided into the superior and inferior bulb pathways, provides input to R-neurons. Superior bulb pathway: Tuberculo-bulbar (TuBu) neurons of lineage DALcl1 (dark blue) project from the lateral domain of the anterior optic tubercle (AOTUI) to the superior bulb (BUs), which then innervate R-neurons (dark red) that project to the anterior and outer central domains of the EB (EBa/oc). Inferior bulb pathway: TuBu neurons of lineage DALcl2 (light blue) project from the intermediate medial domain of the anterior optic tubercle (AOTUim) to the inferior bulb (BUi), which then innervate R-neurons (light red) that project to the inner central and inner posterior domains of the EB (EBic/ip). The anterior bulb (Continued)

**FIGURE 1 | Continued**

pathway is not depicted. Columnar elements of the DM lineages (turquoise), such as E-PG neurons, form recurrent circuitry interconnecting the protocerebral bridge (PB), EB, and gall (GA) of the lateral accessory lobe (LAL). Many other neuron types not shown interconnect the fan-shaped body (FB) and noduli (NO) as well. **(B,C)** Representative examples of columnar and tangential elements of the EB. **(B)** E-PG neuron and **(C)** R2-neuron. Images obtained with permission and adapted from Hanesch et al. (1989). **(D–G)** Confocal z-projections illustrating domains of the bulb and EB, visible with DN-cadherin (DNcad) immunostaining (gray). **(D)** horizontal section; **(E–G)** frontal sections at three different antero-posterior depths. **(D)** Horizontal section (anterior pointing downward) depicting the length of the EB canal (arrow). The EB is situated within an indentation of the FB, located posteriorly. All five EB domains, distinguishable based on DNcad expression levels, are visible: high intensity staining in the anterior-most part of the EB defines the anterior domain (EBa). Posterior to EBa is the inner central domain (EBic) with lower DNcad signal, located medially adjacent to the outer central domain (EBoc) with moderate DNcad signal. Furthest posterior are the inner posterior (EBip) and outer posterior (EBop) domains with low and high intensity DNcad signal, respectively. In this horizontal section, the anterior bulb (BUa) as well as the anterior and posterior regions of the inferior bulb (a/pBUi) are visible, but the superior bulb, located more dorsally, is not. **(E)** Anterior section: the anterior bulb (BUa) and anterior domain of the EB (EBa) are visible. In addition, the anterior-most part of inner central domain (EBic) is also visible (low intensity region proximal to the EB canal). **(F)** Intermediate section: the anterior regions of the superior bulb (aBU) and inferior bulb (aBUi), as well as the inner central (EBic) and outer central (EBoc) domains of the EB are visible. **(G)** Posterior section: the posterior regions of the superior bulb (pBU) and inferior bulb (pBUi), as well as the inner posterior (EBip) and outer posterior (EBop) domains of the EB are visible. Other abbreviations: CRE, crepine; MB, mushroom body; ML, medial lobe; PED, peduncle of the mushroom body. Scale bar represents 25  $\mu\text{m}$  **(D–G)**.

information (TuBu and ring neurons), and circuits that encode and update a representation of heading direction (E-PG and P-EN neurons). In addition, internal state information is likely integrated into the EB network by additional ring neuron subclasses that signal physiological needs such as sleep and hunger drive (Dus et al., 2013; Liu et al., 2016; Park et al., 2016).

To make further inroads in understanding how the EB circuitry operates, a comprehensive knowledge of ring neurons and their upstream and downstream connectivity is required. Ultimately, a comprehensive analysis of single cells and their synaptic contacts on the light and electron microscopy level will yield complete coverage of the EB wiring diagram, and certainly inform our understanding of how EB-related computations are implemented (Zheng et al., 2018). However, a current description of subclass-specific projection patterns using genetic driver lines provides a framework to posit inter-class neural interactions that can then be tested physiologically and/or behaviorally, and will assist future efforts for such high-resolution anatomical maps. To this end, we sought to expand on previous works using this genetic-anatomical approach to more thoroughly describe the EB neuropil (Renn et al., 1999; Young and Armstrong, 2010b; Martín-Peña et al., 2014; Omoto et al., 2017). Gal4 driver lines that label ring neuron subclasses were screened and subsequently distinguished from each other based on defined criteria. Many drivers label populations corresponding to previously identified ring neuron subclasses, in addition to several, yet uncharacterized populations. The novel subclasses were given new names per the historical nomenclature system. Columnar elements were also incorporated into this anatomical framework. Based on the domain innervation pattern of each line, putative interactions between elements within the EB network are proposed. Finally, ring neuron drivers were subjected to the anterograde *trans*-synaptic labeling method, *trans*-Tango (Talay et al., 2017). Ring neurons occupying central domains of the EB commonly display homotypic interactions, such that neurons of a given subclass predominantly form synaptic interactions with other neurons in the same subclass. On the other hand, ring neurons occupying the peripheral domains typically display a larger degree of output into the columnar network.

This highlights a fundamental difference in the connectivity, and potentially the functions, of ring neurons in different domains.

## MATERIALS AND METHODS

### Fly Lines

The following *Drosophila* Gal4 driver lines are from the Janelia Research Campus stock collection (Jenett et al., 2012), and acquired from the Bloomington *Drosophila* Stock Center (BDSC), Bloomington, IN, United States: R31A12, R78B06, R80C07, R28E01, R28D01, R12G08, R84H09, R15B07, R12B01, R59B10, R38H02, R78A01, R14G09. VT063949, VT057232, and VT011965 are Vienna Tile Gal4 driver lines (Tirian and Dickson, 2017) and were acquired from Dr. Barry Dickson. Ring neuron lines were typically identified by visually screening the Janelia FlyLight database<sup>1</sup>. R14G09 was identified by first visually screening the FlyCircuit database<sup>2</sup> for EB innervating neurons, yielding clone ID# VGlut-F-300355 (Chiang et al., 2011), followed by use of the NBLAST (Flycircuit to Gal4 query) search algorithm (Costa et al., 2016). Additional stocks, with citation and availability listed in parentheses: 189Y, c42, c232, c105, c507 (Renn et al., 1999; BDSC), EB1-Gal4 (Young and Armstrong, 2010b), Poxn-Gal4 (Boll and Noll, 2002; provided by Dr. H. Reichert), 10xUAS-mCD8::GFP (BDSC), TPH-Gal4 (Park et al., 2006; provided by Dr. M. Frye), TH-Gal4 (Friggi-Grelin et al., 2003; BDSC), UAS-DenMark::mCherry, UAS-syt.EGFP (Nicolai et al., 2010; BDSC), su(Hw)attP8:HA\_V5\_FLAG\_1 (Nern et al., 2015; BDSC), *trans*-Tango (Talay et al., 2017; provided by Dr. G Barnea).

### Clonal Analysis

Mosaic analysis with a repressible cell marker (MARCM) was conducted to generate heat shock inducible, single-cell clones of ring neurons (Lee and Luo, 1999). Flies of the following genotypes

<sup>1</sup><http://flweb.janelia.org/cgi-bin/flew.cgi>

<sup>2</sup><http://www.flycircuit.tw/>

were utilized: *hsflp/+; FRTG13, UAS-mCD8GFP/FRTG13, tub-GAL80; tub-Gal4/+* or *FRT19A, tub-GAL80, hsflp, UAS-mCD8GFP/elav<sup>C155</sup>-Gal4, FRT19A; UAS-mCD8GFP/+*. GFP-labeled adult single cell MARCM clones were induced at the late first instar/early second instar stage by heat-shocking in a water bath at 38°C for 30–60 min. Larvae were collected after hatching, reared at 18°C, and heat-shocked at different time intervals between 12 and 144 h (double time; corresponding to roughly 6–72 h at 25°C). Heat-shocked larvae were grown to adulthood for subsequent dissection and analysis. Single-cell analysis of R78A01-Gal4, TH-Gal4, TPH-Gal4, and R14G09-Gal4 positive neurons was conducted using the multicolor flip-out method (MCFO) described previously (Nern et al., 2015; Wolff et al., 2015).

## Immunostaining

Three to eight day old female adults were used for all experiments; potential sexual dimorphism would be undetected in this study. Flies were grown at 25°C on standard fly media, in low density bottles on a 12h:12h light/dark schedule. Immunohistochemical procedures were conducted as follows, and are similar to those previously described (Omoto et al., 2017). Adult brains were dissected in phosphate buffered saline (PBS), pH 7.4. Brains were (1) fixed in ice-cold PBS containing 4% EM-grade paraformaldehyde for 2.5–3 h; (2) washed 4× for 15 min each with ice-cold PBS; (3) subjected to cold ethanol-PBS dehydration (5 min washes in 5, 10, 20, 50, 70, 100% EtOH); (4) stored in –20°C overnight; (5) rehydrated using the same cold EtOH series in reverse order; (6) washed 2× 15 min in cold PBS and 2× 15 min washes in cold 0.3% PBT (PBS containing 0.3% Triton X-100); (7) washed in room temperature (RT) 0.3% PBT 4× 15 min; (8) incubated in blocking buffer (10% normal goat serum in 0.3% PBT) for 30 min at RT; (9) incubated in primary antibody, diluted in blocking buffer, at 4°C for three nights; (10) washed 4× 15 min in RT 0.3% PBT; (11) incubated with secondary antibody diluted in blocking buffer at 4°C for an additional three nights; (12) washed 4× 15 min in RT 0.3% PBT and mounted using Vectashield (Vector Laboratories). For 10xUAS-mCD8::GFP panels, native fluorescence of the reporter was used to visualize the neurons. To maximally detect both pre- and post-synaptic neurons in *trans*-Tango experiments, both anti-GFP and anti-DsRed were utilized.

The following antibodies were provided by the Developmental Studies Hybridoma Bank (Iowa City, IA, United States): rat anti-DN-cadherin (DN-EX #8, 1:20), mouse anti-neuroglial (BP104, 1:30). Chicken anti-GFP (Abcam #ab13970, 1:1000) and Rabbit anti-DsRed (Clontech #632496, 1:1000) were also used. We also used rabbit anti-HA (1:300, Cell Signaling Technologies), and mouse anti-V5 (1:1000, Thermo Fisher Scientific).

Secondary antibodies, IgG<sub>1</sub> (Jackson ImmunoResearch; Molecular Probes) were used at the following dilutions: Cy5-conjugated anti-mouse (1:300), Cy3-conjugated anti-rat (1:300). Alexa We used 488-conjugated anti-chicken (1:1000), Alexa 546-conjugated anti-rabbit (1:1000), Alexa 488-conjugated anti-mouse (1:1000) from Thermo Fisher Scientific. Cy5-conjugated anti-rat (1:300) and cy3-conjugated anti-rabbit (1:300) from Abcam were also used.

## Confocal Microscopy and Image Analysis

Samples were mounted primarily in the antero-posterior (A-P) or dorso-ventral (D-V) orientation, and in some cases the postero-anterior (P-A) orientation. D-V orientation required constructing a crevice using two closely neighboring pieces of tape followed by two cover slips, into which the brain can be inserted dorsal-side up. Whole-mounted brains were imaged using confocal microscopy [LSM 700 Imager M2 using Zen 2009 (Carl Zeiss Inc.)]. Series of optical sections were imaged using a 40× oil lens with a numerical aperture of 1.3, a zoom factor of 1.0, at 1.2-μm intervals, and 1024 pixel × 1024 pixel resolution. Digitized images of confocal sections were processed in FIJI (Schindelin et al., 2012<sup>3</sup>). The EB, relative to the rest of the brain, exhibits a tilt on its frontal axis such that the ventral half is oriented anteriorly. We established standard, reproducible views of the EB in both the frontal and horizontal planes (used in all figures) by digitally tilting the z-stack using the “Interactive Stack Rotation” plugin<sup>4</sup>. Antero-posteriorly and dorso-ventrally mounted preparations were digitally tilted such that the canal of the EB was oriented parallel and perpendicular to the z-axis, respectively. In several cases, particularly in cases for z-projections that span large depths (greater than ~75 μm; ex. dorsal *trans*-Tango images), background labeling was manually removed in FIJI to improve visualization of entire neuronal ensembles. Cell counts were conducted manually using the FIJI “Cell Counter” plugin<sup>5</sup>. Cell body clusters on both sides of each brain were counted for at least three samples per driver line. Mean and standard error of the mean was calculated. Schematics were generated in Adobe Illustrator and figures constructed in Adobe Photoshop. Videos were compiled using Camtasia 9.1 with annotations on individual slices made using FIJI “Dotted Line” plugin<sup>6</sup>.

## RESULTS

### Classification of EB Ring Neurons: Criteria and General Considerations

Using Golgi staining to characterize individual CX neuron types in *Drosophila*, the term “ring neuron” was coined by Hanesch et al. (1989), defined as “large-field neurons forming ring-like arborizations around the ellipsoid body canal.” Although “R-neuron” is commonly used as a synonymous abbreviation for “ring neuron,” the latter (full) term was originally used by Hanesch et al. (1989) as an umbrella designation for two major neuron types, R and ExR (“extrinsic ring neurons”). R-neurons represent the most abundant type, with cell bodies located in the anterior cell body rind (also called cortex herein), dorso-laterally of the antennal lobes. ExR-neurons were defined as ring neurons that have “extensive arborizations outside of the EB.” Due to the utility of this distinction to refer to ring neurons derived from

<sup>3</sup><http://fiji.sc/>

<sup>4</sup>[http://imagej.net/Interactive\\_Stack\\_Rotation](http://imagej.net/Interactive_Stack_Rotation)

<sup>5</sup><https://imagej.nih.gov/ij/plugins/cell-counter.html>

<sup>6</sup><https://imagej.nih.gov/ij/plugins/dotted-line.html>

distinct neuroblast lineages (DALv2 = R-neurons; DM3-6 and BAMv1 = ExR-neurons), we re-adopt it for this study (see below; **Figures 5A, 8A**).

For the time being, we adopt and expand upon the historical *Drosophila* ring neuron nomenclature system (i.e., R1, R2, ExR1, etc.), initially introduced by Hanesch et al. (1989) with other studies largely following suit (Renn et al., 1999; Young and Armstrong, 2010b; Omoto et al., 2017). Wolff et al. (2015) developed a formal nomenclature system for neuron types of the PB, in which each cell type was named based on a unique, descriptive collection of identifiers. As more information becomes available, adopting a unified nomenclature system in conjunction with subordinate colloquial terminology, for ring neurons and other neurons comprising the rest of the CX or brain in general, may be most suitable (Franconville et al., 2018; Wolff and Rubin, 2018). We propose that this prospective system would ideally incorporate lineage classification as one of these identifiers, since the fly brain is inherently organized into structurally and developmentally defined clonal units.

In most cases, the Gal4 drivers that label the ring neurons described in this study were visually screened from the Janelia (Jenett et al., 2012) or Vienna Tiles (Tirian and Dickson, 2017) collections and subsequently stained with the global neuropil marker DN-cadherin. Drivers were classified as labeling a unique ring neuron subclass based on the following criteria: (1) the EB DN-cadherin domain occupied by the circular, predominantly axonal, arbors, (2) the trajectory and morphology of said projections, and (3) the location of their presumed dendritic proximal neurites, typically microglomeruli in the bulb (BU) or fibrous neurites in the lateral accessory lobe (LAL).

Altogether, we identified fifteen unique ring neuron subclasses: eleven R-neuron and four ExR-neuron subclasses. This expands the catalog from six R-neuron (R1, R2, R3, R4m, R4d, R5) and two ExR-neuron (ExR1 and ExR2) subclasses, from previous reports (Hanesch et al., 1989; Renn et al., 1999; Young and Armstrong, 2010b; Omoto et al., 2017). However, it is critical to note a caveat of this study: each driver labels a population of neurons which were not anatomically evaluated on a single-cell basis, as has been done for the neurons innervating the PB (Wolff et al., 2015). Indeed, multicolor-flip out analysis (MCFO) of some ring neuron drivers from this study yielded qualitatively distinct anatomical subtypes, even within a superficially homogenous population (data not shown). Therefore, although this study significantly expands upon the cohort of known ring neuron subclasses, in the absence of higher-resolution methods (single-cell light microscopy, TEM reconstructions) and supplementary genetic/physiological evidence, the precise diversity of ring neuron subclasses is still underestimated. Nonetheless, this study provides a more complete catalog and explicit criteria with which ring neuron subclasses can be anatomically defined. These criteria may be used as a framework to define new subclasses identified in subsequent studies.

One supplementary objective of this study is to resolve discrepancies in the literature regarding ring neuron subclasses, a consequence of somewhat undefined criteria and lack of spatial resolution. We have reevaluated previously published driver lines based on the proposed criteria and have found that oftentimes,

a given ring neuron subclass has been called distinct names in different studies. Alternatively, a previously unidentified subclass has been assumed to be one of the preexisting subclasses because it appeared similar. When examining each subclass below, we will refer to pertinent examples of this, and provide data to reevaluate these comparisons based on our criteria.

## R-Neurons: Lineage DALv2/EBa1

The most abundant ring neuron type is the R-neurons, whose cell bodies are located dorso-laterally of the antennal lobes and exhibit projections that extend dorso-posteriorly, branching off localized neurites into the BU or LAL, enter the lateral ellipsoid fascicle [(LE; Pereanu et al., 2010; Strausfeld, 2012; Lovick et al., 2013); also called the “isthmus tract” (Ito et al., 2014)], and via a circular process, terminates medially into the EB (**Figures 2, 3**). In the EB, distal neurites of R-neurons either project centrifugally (“inside-out”; **Figure 2**) or centripetally (“outside-in”; **Figure 3**). Clonal analysis of fly brain lineages revealed a single paired type I neuroblast that generates R-neurons called DALv2 (Wong et al., 2013; Omoto et al., 2017), also called EBa1 (Ito et al., 2013; Yu et al., 2013). The driver Poxn-Gal4 (Boll and Noll, 2002; data not shown), which labels the majority of (but possibly not all) DALv2 R-neurons, can, at first approximation, be used to estimate the total number of R-neurons. Quantification of these cells reveals  $158 \pm 9$  R-neurons per brain hemisphere (PBH). Despite the aforementioned caveats, the following catalog of R-neuron drivers is likely close to comprehensive, considering that summation of the neurons from each R-neuron driver (11 lines) totals  $\sim 176$  cells PBH (see below). In the following sections, we summarize the neuroanatomy of Gal4 lines that label unique R-neuron patterns.

### R1

R1 neurons (Renn et al., 1999), here labeled by the driver 31A12-Gal4 (**Figure 2A** and **Supplementary Movies 1, 2**;  $13 \pm 2$  neurons PBH), are among the minority of R-neurons that do not form glomerular dendritic branches in the BU, but instead connect to the adjacent LAL. Here, terminal branches form a tuft of fine fibers spreading along the lateral surface of the LAL, ventrally and posteriorly adjacent to the gall (GA; **Figures 2A1–A4**). Distal fibers of R1 continue medially along the LE, curve around the anterior surface of the EB and, after entering the central canal, project posteriorly. Terminal distal branches densely fill a narrow volume within the outer posterior domain of the EB (EBop) which lines the boundary between EBop and the inner posterior domain (EBip) (**Figures 2A5,6**). The identical pattern is labeled by c105 (Renn et al., 1999; **Supplementary Figure 1A**). The expression of constructs that are specifically targeted toward the dendritic and axonal compartments of neurons (UAS-DenMark, UAS-syt.EGFP; Nicolai et al., 2010) suggest that proximal projections to the LAL are exclusively postsynaptic/dendritic, and distal ones terminating in the EB are predominantly axonal (**Supplementary Figure 2**).

### R2

R2 neurons, defined by Hanesch et al. (1989) are labeled here by 78B06-Gal4 (**Figure 2B** and **Supplementary Movies 3, 4**;

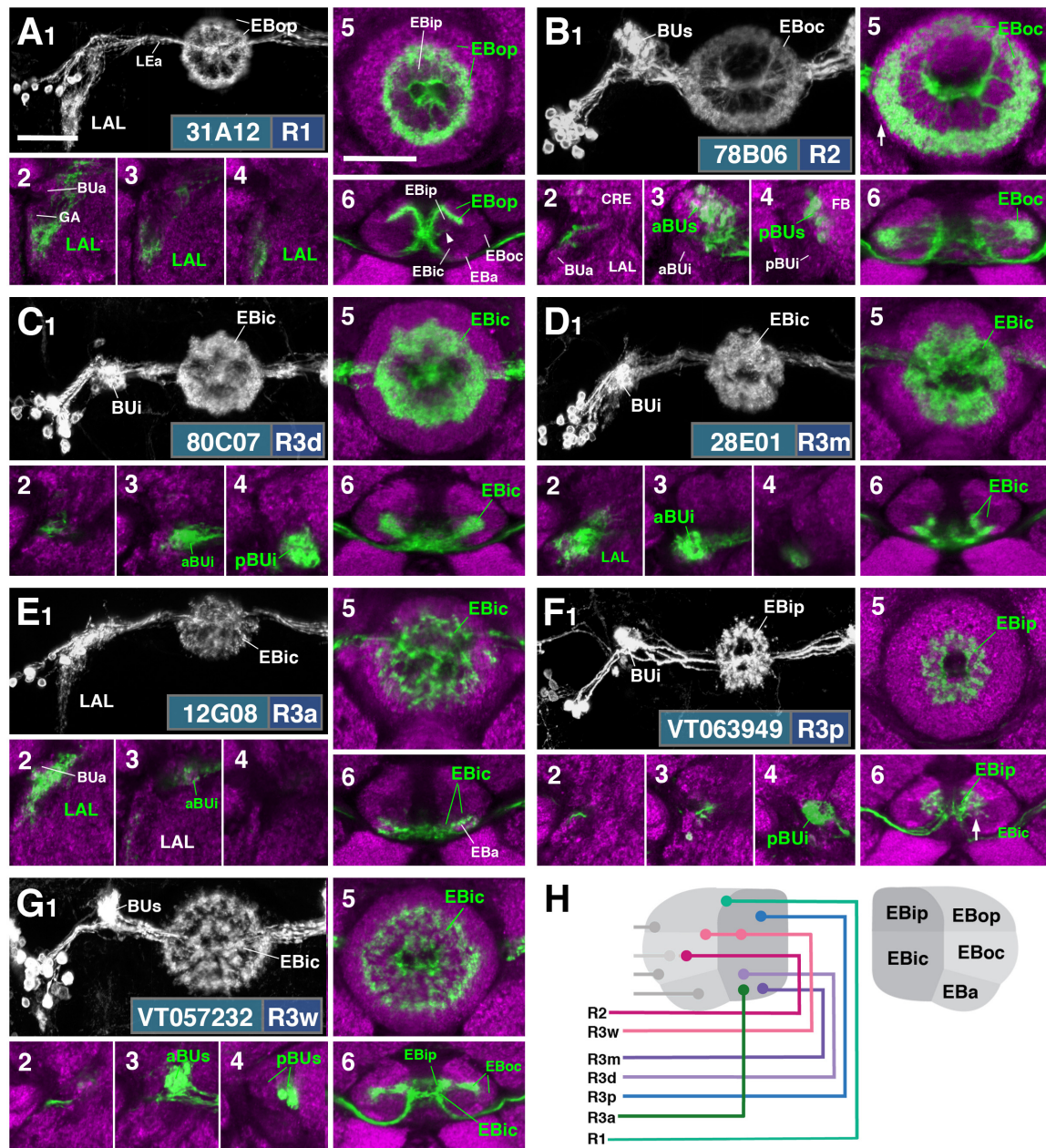


**FIGURE 2 |** R-neuron subclasses of lineage DALv2/EBa1 with centrifugal arborizations. **(A–G)** Confocal z-projections of Gal4 drivers that label distinct R-neuron subclasses. Each lettered, six-paneled module corresponds to an individual driver labeled with 10xUAS-mCD8::GFP. Within each module, Top Left (1) is a grayscale z-projection of the specific subclass (cell bodies on left), and its corresponding driver and name in the bottom right corner. Large white annotations designate the primary domains of innervation by the subclass. In remaining module panels, the GFP-labeled neurons are shown in green; neuropil is labeled with anti-DN-cadherin (magenta). Bottom left panels (2–4) are three frontal sections of the bulb at different antero-posterior depths (as described in **Figure 1**); from left to right: anterior section containing BUa, intermediate section containing aBUs and aBUi, posterior section containing pBUs and pBUi. Some subclasses (R1 and R3) innervate the LAL rather than the bulb, in which case the same sections are shown at a more ventral position. Top Right (5) is a higher magnification, frontal view of the EB at an antero-posterior level (anterior, intermediate, or posterior) that highlights the circular arbor of a given driver most clearly. Bottom Right (6) is a horizontal section visualizing all five DN-cadherin positive domains. Highlighted in large green text is the domain predominantly innervated by the R-neuron subclass; smaller green text signifies additional regions of innervation. Small white text in all panels denotes relevant spatial landmarks. **(A1–6)** R31A12-Gal4 (R1). **(A1–5)** Refer to **Supplementary Movie 1**. **(A1)** R1 projects from the LAL to EBop. For all DALv2 R-neurons, the anterior component of the lateral ellipsoid fascicle (LEa) comprises the bridge between proximal and distal, annular neurites. **(A2–4)** Ventral neurites of R1 extend in the lateral LAL, medially adjacent of the gall (GA). **(A5)** Posterior EB section. **(A6;** refer to **Supplementary Movie 2**) R1 neurites in the EB line the anterior-most border of EBop, along the EBip–EBop interface. Additional, very small protrusions emanate from canal projections, along the EBip–EBic interface (arrowhead; **A6**). **(B1–6)** R78B06-Gal4 (R2). **(B1–5)** Refer to **Supplementary Movie 3**. **(B1)** R2 projects from BUs to EBoc. **(B2)** No significant innervation in BUa; GFP signal corresponds to bypassing neurites. **(B3)** R2 neurons exhibit most of their

(Continued)

**FIGURE 2 |** Continued

microglomeruli in aBUs, but **(B4)** also some in pBUs. **(B5)** Intermediate EB section; arrow indicates peripheral fringe of EBoc which is not innervated. **(B6;** refer to **Supplementary Movie 4**) R2 exhibits restricted innervation of EBoc; GFP signal in EBic is passing neurites. **(C1–6)** R80C07-Gal4 (R3d – *distal*). **(C1–5)** Refer to **Supplementary Movie 5**. **(C1)** R3d projects from BUI to EBic. **(C2)** No significant innervation in BUa; GFP signal corresponds to bypassing neurites. **(C4)** R3d neurons exhibit most of their microglomeruli in pBUi, but **(C3)** also some in aBUi. **(C5)** Intermediate EB section. **(C6;** refer to **Supplementary Movie 6**) R3d fills most of EBic. **(D1–6)** R28E01-Gal4 (R3m – *medial*). **(D1–5)** Refer to **Supplementary Movie 7**. **(D1)** R3m projects from BUI to EBic. **(D3)** R3m neurons exhibit most of their microglomeruli in aBUi, but **(D2)** possibly also extend fibrous projections in the LAL, adjacent to BUa. **(D4)** No significant innervation in pBUs/i. **(D5)** Anterior EB section. **(D6;** refer to **Supplementary Movie 8**) R3m fills complementary region of EBic relative to R3d. **(E1–6)** R12G08-Gal4 (R3a – *anterior*). **(E1–5)** Refer to **Supplementary Movie 9**. **(E1)** R3a projects from the LAL to EBic. **(E2)** The LAL projections of R3a neurons are more closely adjacent to BUa, than those of R1 neurons **(A2)**, and **(E3)** may also exhibit very sparse projections in aBUi. **(E4)** No significant innervation in pBUs/i. **(E5)** Anterior EB section. **(E6;** refer to **Supplementary Movie 10**) The EB neurites of R3a surround EBa. **(F1–6)** VT063949-Gal4 (R3p – *posterior*). **(F1–5)** Refer to **Supplementary Movie 11**. **(F1)** R3p projects from BUI to EBip. **(F2,3)** No significant innervation in BUa and aBUs/i; GFP signal corresponds to bypassing neurites. **(F4)** R3p neurons exhibit their microglomeruli in pBUi. **(F5)** Posterior EB section. R3p neurites in the EB densely fill EBip, but **(F6;** refer to **Supplementary Movie 12**) also appear to project anteriorly, penetrating EBic (arrow). **(G1–6)** VT057232-Gal4 (R3w – *wide*). **(G1–5)** Refer to **Supplementary Movie 13**. **(G1)** R3w projects from BUs to EBic. **(G2)** No significant innervation in BUa; GFP signal corresponds to bypassing neurites. **(G3,4)** R3w neurons exhibit their microglomeruli in aBUs and pBUs. **(G5)** Posterior EB section. **(G6;** refer to **Supplementary Movie 14**) R3w neurites line the posterior border of EBic, and extend into EBip. Neurites also extend distally toward EBoc, and may encroach on it. **(H)** Schematized overview of EB domain innervation patterns of centrifugally projecting R-neurons. CRE, crepine. Scale bars represent 25  $\mu\text{m}$  **(A–G)**.

23  $\pm$  2 neurons PBH). Other drivers predominantly labeling this subclass are c42 (**Supplementary Figure 1B**), introduced by Renn et al. (1999), and EB-1 (Young and Armstrong, 2010b; Seelig and Jayaraman, 2013; Thran et al., 2013; **Supplementary Figure 1C**). R2 comprises outer R-neurons with distal, axonal endings branching throughout most of the outer central domain of the EB (EBoc; **Figures 2B1,5,6**). Only a narrow fringe along the periphery of EBoc is devoid of R2 terminals (**Figure 2B5**; arrow). This fringe is innervated by R4d (see below). R2 axons reach their destination by following the LE around the anterior surface of the EB, entering the central canal and then projecting centrifugally toward EBoc (**Figures 2B5,6**). By this criterion they differ from the outer ring neuron subclass R4m (**Figure 3B**), which projects to the same domain, but reaches it in a centripetal fashion (see below). Proximal dendrites of R2 form club-shaped glomerular endings in the medial two-thirds of the superior bulb (BUs; **Figures 2B3,4**).

### R3 (Distal, Medial, Anterior, Posterior, Wide)

The former R3 subclass of inner ring neurons can be broken up into at least five subclasses, R3d, R3m, R3a, R3p, R3w, defined by their axonal projections to distinct regions within the inner central (EBic) and inner posterior (EBip) domains of the EB. R3d neurons, marked by the driver 80C07-Gal4 (**Figure 2C** and **Supplementary Movies 5, 6**; 36  $\pm$  1 neurons PBH), project along the LE toward the anterior EB surface, turn posteriorly into the central canal and from there spread centrifugally throughout EBic (**Figures 2C5,6**). They spare a small medial and anterior portion of EBic, which are innervated in a partially overlapping fashion by the subclasses R3m (**Figures 2D5,6** and **Supplementary Movies 7, 8**; 21  $\pm$  1 neurons PBH) and R3a (**Figures 2E5,6** and **Supplementary Movies 9, 10**; 11  $\pm$  0 neurons PBH), respectively. Microglomerular dendritic endings of R3d fill the posterior region of the inferior bulb (pBUi; **Figure 2C4**). A few additional microglomeruli are observed in the dorso-medial part of the anterior region of the inferior bulb (aBUi), leaving the rest of aBUi empty (**Figure 2C3**). Dendritic projections of R3m [marked by 28E01-Gal4 in **Figure 2D**,

and likely by 28D01-Gal4 (**Supplementary Figure 1D**; referred to as “R1” in Ofstad et al., 2011)] and R3a (12G08-Gal4; **Figure 2E**) differ from that of R3d: R3m dendrites are relatively confined to aBUi (**Figure 2D3**), and R3a may send very few, fibrous dendrites to aBUi, directing most of its dendrites to a small region near the dorso-lateral surface of the LAL, ventromedially adjacent to the anterior bulb (BUa; **Figures 2E1–3**). This “non-canonical” dendritic projection (no glomerular synapses; targeting areas outside the BU) puts R3a in close proximity to R1 (see above). However, the LAL territory innervated by R1 appears larger, and is located more postero-medially, than the one targeted by R3a (compare **Figures 2A1–4** and **E1–4**).

The inner ring neuron subclass R3p, marked by VT063949-Gal4 (**Figure 2F** and **Supplementary Movies 11, 12**; 9  $\pm$  0 neurons PBH), has axonal projections predominantly restricted to the inner posterior domain (EBip) of the EB, largely non-overlapping with the projection of R3d/m/a (**Figures 2F5,6**). Some small projections extend anteriorly, encroaching on EBic (**Figure 2F6**; arrow). Dendritic branches comprise a main conglomerate of endings located in the dorsal part of pBUi (**Figure 2F4**), a region not occupied by dendritic endings of R3d (compare to **Figure 2C4**).

Finally, the arborization pattern of ring neurons called R3w, marked by VT057232-Gal4 (**Figure 2G** and **Supplementary Movies 13, 14**; 27  $\pm$  2 neurons PBH), comes closest to that of the neuron subclass originally designated “R3” by Hanesch et al. (1989). Like all other R3 neurons listed above, R3w neurons project axons past the anterior surface of the EB into the canal, from where they spread centrifugally (**Figures 2G1,5,6**). However, terminal branches are given off centrally, near the boundary between EBic and EBip, as well as more peripherally, in the inner part of EBoc (**Figures 2G5,6**). Glomerular dendritic endings occupy a medial region within the BUs (**Figures 2G3,4**).

Driver lines expressed in inner ring neurons (“R3”) described previously may represent composites marking two or more different neuron subclasses. For example, 189y (Renn et al., 1999; **Supplementary Figure 1E**) and 84H09 (Omoto et al., 2017; **Supplementary Figure 1F**) include dendritic and axonal

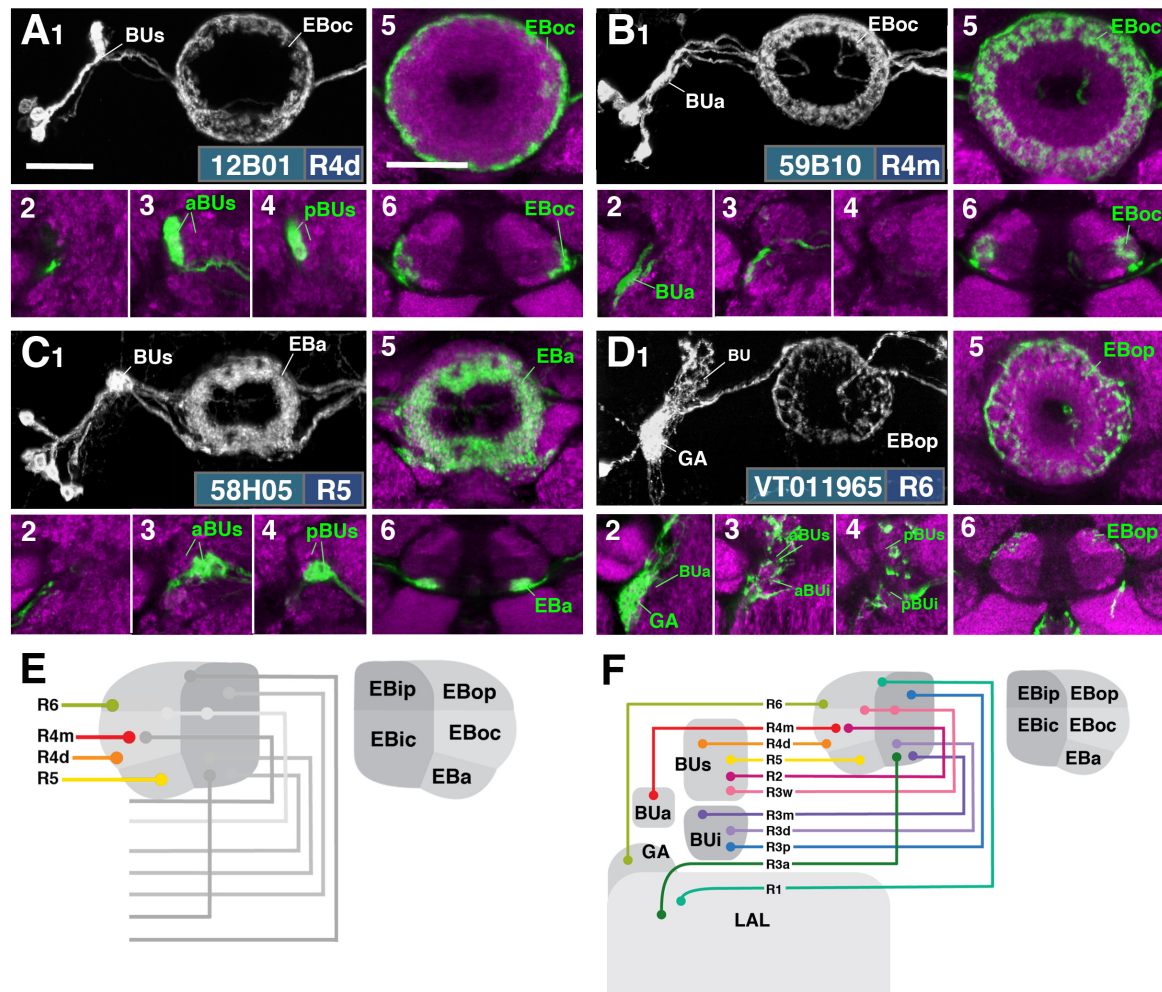


**FIGURE 3** | R-neuron subclasses of lineage DALv2/EBa1 with centripetal arborizations. **(A–D)** Similar modular format of panels as described in legend for **Figure 2**. **(A1–6)** R12B01-Gal4 (R4d – distal). **(A1–5)** Refer to **Supplementary Movie 15**. **(A1)** R4d projects from BUs to EBoc. **(A2)** No significant innervation in BUa; GFP signal corresponds to bypassing neurites. **(A3,4)** R4d neurons exhibit their microglomeruli in aBUs and pBUs. **(A5)** Intermediate EB section. **(A6)**; refer to **Supplementary Movie 16** R4d neurites line the distal-most border of EBoc, and typically extend from posterior edge of EBa to the anterior edge of EBop. **(B1–6)** R59B10-Gal4 (R4m – medial). **(B1–5)** Refer to **Supplementary Movie 17**. **(B1)** R4m projects from BUa to EBoc. **(B2–4)** Innervation only in BUa; GFP signal in aBUs/i corresponds to bypassing neurites. **(B5)** Intermediate EB section. **(B6)**; refer to **Supplementary Movie 18** R4m neurites innervate EBoc. **(C1–6)** R58H05-Gal4 (R5). **(C1–5)** Refer to **Supplementary Movie 19**. **(C1)** R5 projects from BUs to EBa. **(C2)** No significant innervation in BUa; GFP signal corresponds to bypassing neurites. **(C3,4)** R5 neurons exhibit their microglomeruli in aBUs and pBUs. **(C5)** Anterior EB section. **(C6)**; refer to **Supplementary Movie 20** R5 neurites innervate EBa. **(D1–6)** VT011965-Gal4 (R6). **(D1–5)** Refer to **Supplementary Movie 21**. **(D1)** R6 projects from the gall (GA) to EBop. **(D2–4)** R6 neurites are highly dense in the GA, but also diffusely innervate all domains of BU. **(D5)** Posterior EB section. **(D6)**; refer to **Supplementary Movie 22** R6 form sparse projections in the posterior boundary of EBop and extend fine processes anteriorly into EBop. **(E)** Schematized overview of EB domain innervation patterns of centripetally projecting R-neurons. **(F)** Complete overview of the connectivity between the EB and its associated neuropil compartments via R-neurons (Summary of **Figures 2, 3**). Scale bars represent 25  $\mu\text{m}$  (**A–D**).

territories of R3d and R3p, targeting EBic and EBip, and much of BUi, including the dorsal territory labeled by the R3p. c232 and c507 (Renn et al., 1999; **Supplementary Figures 1G,H**), as well as 15B07-Gal4 (Ofstad et al., 2011; **Supplementary Figure 1I**) may represent a composite of R3d, R3p, and R4d, targeting EBic, EBoc, and EBip. The peripheral fringe, labeled by R4d (see below), is also present. Accordingly, most of BUi (including the dorsal R3p-associated region) and the lateral part of BUs (characteristic of R4d) are labeled by c232, c507, and 15B07-Gal4. Considering that several driver lines appear to exhibit shared R3d

and R3p innervation patterns, it is also possible that presumably composite lines may mark a distinct subclass of ring neurons that individually branch in both domains; clonal analysis is required to address this possibility.

**Figure 2H** provides a schematic overview of the innervation patterns of centrifugal R-neurons into domains of the EB.

### R4 (Distal and Medial)

Two subclasses of outer ring neurons already described in the existing literature are R4d and R4m. Axons of R4d

(Renn et al., 1999), here specifically labeled by 12B01-Gal4 (**Figure 3A** and **Supplementary Movies 15, 16**;  $8 \pm 0$  neurons PBH), reach the periphery of the EB from where they centripetally project very short terminal tufts into the peripheral fringe of EBoc. Dendritic branches form glomerular synapses confined to the lateral part of BUs (**Figures 3A3,4**). R4m (Renn et al., 1999; here labeled by 59B10-Gal4) has similar axonal projections that penetrate the EB in a centripetal fashion. However, tufts of terminal branches are longer, filling the entire EBoc (**Figures 3B5,6** and **Supplementary Movies 17, 18**;  $11 \pm 3$  neurons PBH). The restricted dendritic projection into BUa is highly characteristic of R4m (**Figure 3B2**).

## R5

In a previous paper (Omoto et al., 2017) we described an additional subclass of outer ring neurons called R5, labeled by 58H05-Gal4, which specifically targets the small, anterior EB domain (EBa; **Figure 3C** and **Supplementary Movies 19, 20**;  $14 \pm 1$  neurons PBH). Axons of R5 approach the antero-lateral surface of the EB, and project short terminal branches centripetally into EBa (**Figures 3C5,6**). Dendritic terminals are confined to BUs, like those of the other outer ring neuron subclasses (R2 and R4d), but occupy a small distinct locus located ventromedially (**Figures 3C3,4**). The driver 38H02-Gal4 has been described in previous works as a subset of R4 neurons (Ofstad et al., 2011; Dus et al., 2013; Park et al., 2016), but reflects a composite marker of R5 in addition to R4m (**Supplementary Figure 1J**), with axonal projection into EBoc and EBa (**Supplementary Figures 1J1–3**), and dendritic endings in BUa and the ventromedial part of BUs (**Supplementary Figures 1J4–6**). R5 has been referred to as “R2” or an “R2 subset” in previous works (Lin et al., 2013), particularly in the field of sleep regulation (Liu et al., 2016; Donlea et al., 2018), but is distinct from R2 as defined in classical works and herein (Hanesch et al., 1989; Renn et al., 1999). R2 was originally described to have a centrifugal projection pattern innervating the outer ring, whereas R5 in the current study displays a centripetal innervation pattern.

## R6

We identified driver line VT011965-Gal4 as being expressed in a small number of DALv2 R-neurons, a subclass we refer to as R6 (**Figure 3D** and **Supplementary Movies 21, 22**;  $2 \pm 0$  neurons PBH). Distal neurites of these neurons approach the EB peripherally (centripetal projection) and form a sparse mesh along the posterior and postero-lateral boundary of EBop (**Figures 3D1,5,6**). They also display short branches that extend anteriorly into EBop (**Figure 3D6**). Proximal neurites have a unique projection pattern, first forming dense branches within the GA, and then continuing into the BU, where they show a web-like innervation reaching throughout BUa, BUi, and BUs (**Figures 3D2–4**).

**Figure 3E** provides a schematic overview of the innervation patterns of centripetal R-neurons into domains of the EB; **Figure 3F** provides a complete overview of the connectivity between the EB and its associated neuropil compartments via R-neurons.

We hypothesized that the different DALv2 subclasses are sublineages, consisting of neurons born at different time points. To address this hypothesis, we induced MARCM clones (Lee and Luo, 1999) using a pan-neuronal driver (tub-Gal4 or *elav*<sup>C155-Gal4</sup>) at defined developmental stages between 20 and 144 h (reared at 18°C) after hatching. Depending on where in the lineage the recombination event occurs, three types of clones [multi-cell or two-cell neuroblast clone, one-cell ganglion mother cell (GMC) clone] appear (**Figure 4A**). In a collection of GMC clones we found that early clone induction (20–48 h) produced exclusively R4m ring neurons (**Figures 4B,C**). By contrast, induction at 48–72 h and 72–96 h resulted in a small fraction of R4m clones (approximately 20% at 48–72 h, and 10% at 72–96 h). Instead, we predominantly find R5, R4d, and R3 neurons (**Figures 4B,D**). R3 neuron subclasses are never seen in early clones (20–48 h), and form the only type of clone induced at later time stages (96–144 h; **Figures 4B,E**); 60% of the clones produced at intermediate time points belong to the R3 subclasses. These data indicate that birthdates of ring neurons differ systematically, and suggest that anatomically defined subclasses of R-neurons are indeed sublineages of DALv2.

## Posterior ExR-Neurons: Lineages DM3–6

Aside from the above described DALv2 neurons, we also observe an additional type of ring neurons. Given their widespread arborization outside the EB, we classify them as extrinsic ring neurons (ExR), in accordance with Hanesch et al. (1989) who introduced this distinction. At least three subclasses of ExR-neurons with cell bodies located in the posterior brain cortex were recognized, and we refer to this group as the posterior ExR-neurons. Based on soma location and axonal projection these cells form part of the type II lineages DPMpm2, CM4, CM3, and CM1, commonly known as DM3–6. Thus, posterior ExR-neurons share a characteristic projection along the medial equatorial fascicle (MEF), which carries long axons from the posterior cortex to the LAL, or the longitudinal superior medial fascicle (loSM), which extends from the posterior cortex to the superior protocerebrum (Pereanu et al., 2010; Wong et al., 2013; Ito et al., 2014; **Figure 5A**). Fibers of large subsets of neurons belonging to lineages CM1 (DM6), CM3 (DM5), and CM4 (DM4) make up the bulk of the MEF, whereas DPMpm2 (DM3) extends along the loSM (Pereanu and Hartenstein, 2006; Ito et al., 2013; Lovick et al., 2013; Wong et al., 2013; Yu et al., 2013).

## ExR1

The first subclass of ExR-neurons has been dubbed recently as “helicon cells” (Donlea et al., 2018), and can be visualized by the driver line 78A01-Gal4. Projecting anteriorly along the MEF, helicon axons reach the bulb (BU) and form ultra-dense arborizations in all partitions of this compartment (**Figure 5C**). Three fiber bundles continue from the BU toward the FB, EB, and GA of the LAL, respectively. The fiber bundle toward the FB exits BUs in the dorso-medial direction and fans out into a plexus of terminal fibers that spread along the anterior edge of the FB roof (layer 8 after Wolff et al., 2015; **Figures 5D,E**). The fiber bundle destined for the EB follows the LE medially. Terminal fibers form a fine web surrounding the surface of

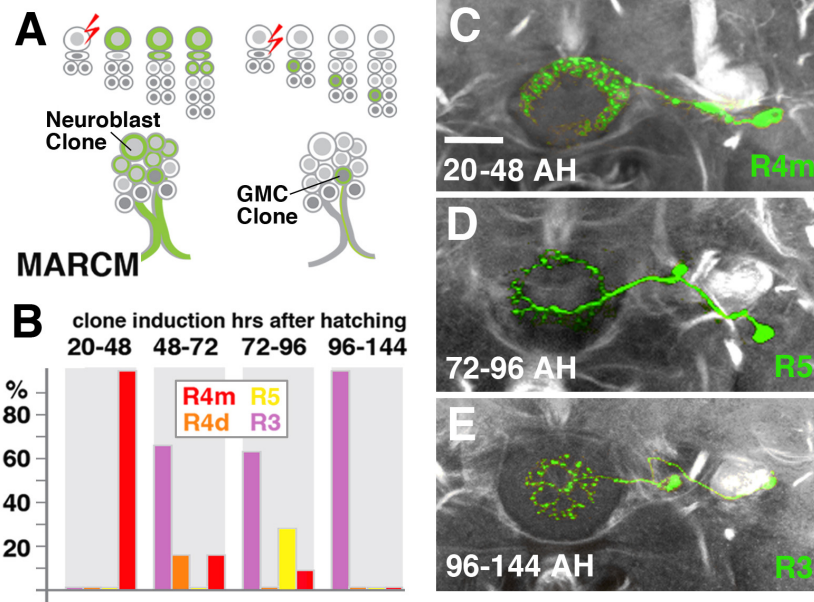


**FIGURE 4 |** R-neuron subclasses represent sublineages of DALv2. **(A)** Schematized overview of MARCM clone induction and resultant clone categories. Neuroblast clones result in labeling of the entire lineage from induction onward; ganglion mother cell (GMC) clones result in singly-labeled neurons. **(B)** Histogram of single cell clone R-neuron subclasses generated by temperature shifts during distinct time windows throughout larval development. A total of 33 single cell clones were generated, % reflect the proportion of clones of a given subclass generated during a given time window. **(C–E)** Representative clones (green) from three time windows after hatching (AH). Axon tracts labeled by anti-Neuroglian (gray). **(C)** R4m. **(D)** R5. **(E)** R3. Scale bars represent 25  $\mu$ m **(C–E)**.

the EB. In addition, endings are concentrated in EBa and EBic (**Figures 5C,E**). A third contingent of fibers projects from BUa toward antero-laterally and densely innervates the GA of the LAL (**Figure 5B**). Single cell analysis of 78A01-Gal4 using the multi-color flip out (MCFO) technique reveals that the innervation pattern of an individual ExR1 neuron reflects that of the entire population (**Figures 5F–I**). Based on the striking morphological similarity, helicon cells likely correspond to the first type of extrinsic R-neuron (ExR1) as defined in Hanesch et al. (1989) (**Figure 21A** in Hanesch et al., 1989; **Figure 12B** in Young and Armstrong, 2010b; **Figure 4A** in Donlea et al., 2018). Based on their cell body position and projection along the MEF, ExR1 can be attributed to the lineages DM4–6, but cannot be assigned to a specific lineage in the absence of further clonal analysis.

### ExR2

The PPM3 group of dopaminergic neurons described in previous works encompasses the next subclass of posterior ExR-neurons (**Figure 6**), and can be visualized by TH-Gal4 (Friggi-Grelin et al., 2003). PPM3 is comprised of 8–9 cells whose bundled axons project anteriorly along the MEF, and form part of lineages DM4 and/or DM6 (Ren et al., 2016; Hartenstein et al., 2017). Reaching the level of the FB, PPM3 neurons branch out and innervate different compartments within the central complex (CX) and adjacent neuropils, including the BU and lateral surface of the LAL, the anterior inferior protocerebrum [also called crepine (CRE); Ito et al., 2014], and the superior medial protocerebrum

(SMP; Hartenstein et al., 2017; **Figures 6A–D**). Single cell clones revealed at least three different types:

- (1) PPM3 neurons innervating the EB, BU, and lateral surface of the LAL (including the GA; **Figures 6E–H**; called PPM3-EB in the following). The PPM3-EB axon projects along the LE and enters EB at a dorso-lateral position (green, **Figure 6F**). Terminal arborizations are concentrated in EBop (**Figure 6H**). Additional branches reach superior and inferior partitions of both ipsi- and contralateral bulbs (**Figure 6F**). Note that within the BU, unlike most DALv2 ring neurons (see **Figures 2, 3**) or the afferent TuBu neurons (Omoto et al., 2017), terminal PPM3-EB branches do not end in large microglomerular structures, but form thin, highly branched endings. Due to its EB innervation, we refer to these neurons as the ExR2 subclass. Like PPM3-EB, ExR2 as defined by Hanesch et al. (1989) also contains a caudal innervation pattern in the EB, but a direct correspondence is difficult to make since the cell from this study was not fully reconstructed and the ring neuron from lineage BAMv1 also innervates the same EB region (see below).
- (2) At least two subtly different kinds of PPM3 neurons innervating FB, NO, LAL, CRE, and SMP exist, one of them shown in **Figures 6E–H** (magenta; PPM3-FB). This cell arborizes in the ventral layers (2–3, after Wolff et al., 2015) of the FB, and the intermediate noduli (NO2). Separate branches project to the lateral surface of the LAL, where projections partially overlap with those of PPM3-EB (green;

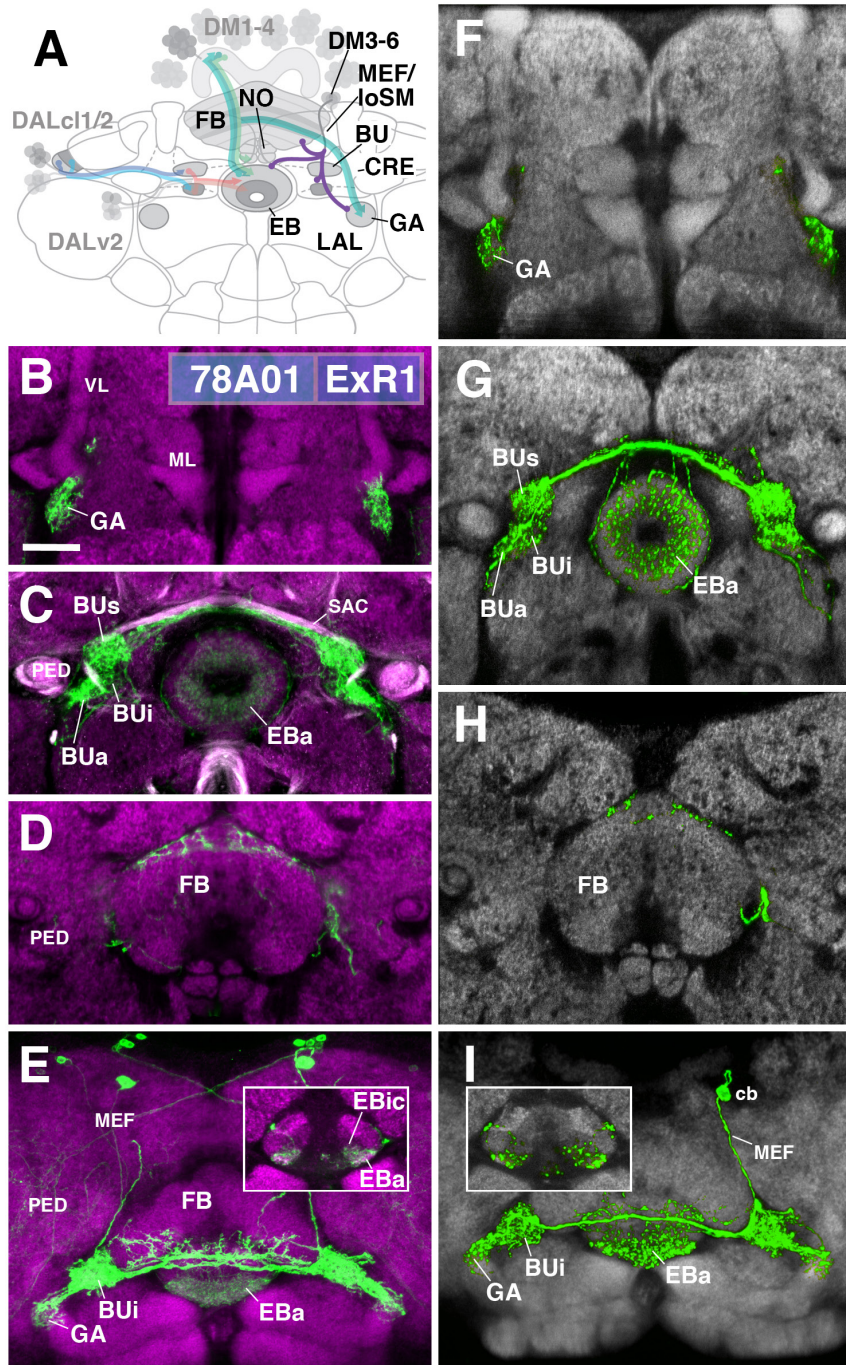


**FIGURE 5 |** ExR1-neurons: posterior extrinsic ring neurons of lineages CM4, CM3, CM1/DM4-6. **(A)** Schematized overview of interacting neuronal populations of the EB from **Figure 1**, now including posterior ExR-neuron subclasses of lineages CM4, CM3, CM1, DPMpm2/DM3-6 (refers also to **Figures 6, 7**). **(B–E)** Confocal z-projections of R78A01-Gal4 driver that labels ExR1-neurons. Neurons labeled with 10xUAS-mCD8::GFP (green). Neuropil labeled by anti-DN-cadherin (magenta). Top three rows correspond to frontal sections at three different antero-posterior depths; from top to bottom: anterior section containing the gall (GA)/LAL, intermediate section containing the EB and bulbs (BU), posterior section containing the FB and noduli (NO). Bottom (fourth) row is a horizontal section visualizing the length of the EB canal. Larger white annotations denote arborization-containing domains of interest; smaller white annotations represent spatial landmarks. Inset in panel **(E)** depicts dorsal view of the EB; R78A01-Gal4 innervates EBa and the anterior part of EBic. **(F–I)** Confocal z-projections of individually labeled cells generated by MCFO using 78A01-Gal4. Four panels depict the same sections and are organized in the same fashion as in panels **B–E**. Neuropil labeled by anti-DN-cadherin (gray). Much like the R78A01-positive population, an individual ExR1 neuron innervates **(F)** the GA and **(G)** all BU partitions on both sides, along with EBa. **(H)** Additional innervation includes the dorsal roof of the FB. **(I)** Dorsal view illustrates that the cell body (cb) of an individual cell, located in the posterior cortex, sends a projection along the medial equatorial fascicle (MEF) and arborizes in both EBa and EBic (inset). CRE, crepine; loSM, longitudinal superior medial fascicle; ML, medial lobe; VL, vertical lobe; PED, peduncle of the mushroom body; SAC, superior arch commissure. Scale bars represent 25  $\mu$ m **(B–I)**.

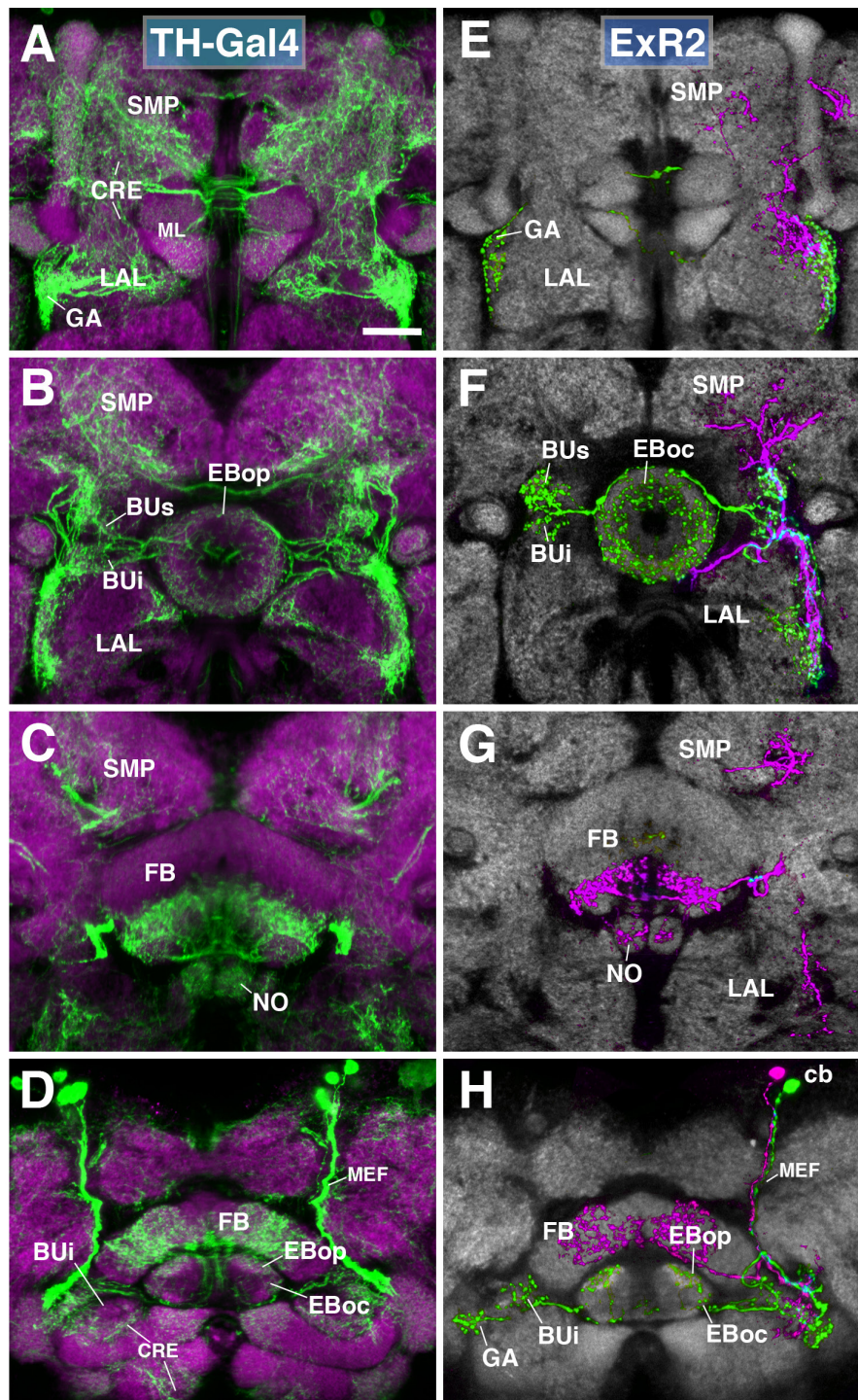


**FIGURE 6** | ExR2-neurons: posterior extrinsic ring neurons of lineages CM4, CM3, CM1/DM4-6. **(A–D)** Panel format similar to **Figures 5B–E**. Confocal z-projections of the TH-Gal4 driver that labels all dopaminergic neurons, including ExR2-neurons. **(E–H)** Confocal z-projections of individually labeled cells generated by MCFO using TH-Gal4. Four panels depict the same sections and are organized in the same fashion as in panels **(A–D)**. Neuropil labeled by anti-DN-cadherin (gray). **(E,F)** Green cell is ExR2 (PPM3-EB dopaminergic neuron); a single PPM3-EB innervates the gall (GA), lateral region of the LAL, and all BU partitions on both sides (BUa is not shown). **(H)** Additional innervation includes EBop, and sparsely EBoc. Magenta cell is not an ExR-neuron (PPM3-FB dopaminergic neuron). Annotation format is identical to that of panels **A–D**. **(H)** Dorsal view illustrates that the cell body (cb) of an individual ExR2-neuron is located in the posterior cortex and projects along the MEF. CRE, crepine; FB, fan-shaped body; ML, medial lobe of the mushroom body; NO, noduli; SMP, superior medial protocerebrum. Scale bars represent 25  $\mu\text{m}$  **(A–H)**.

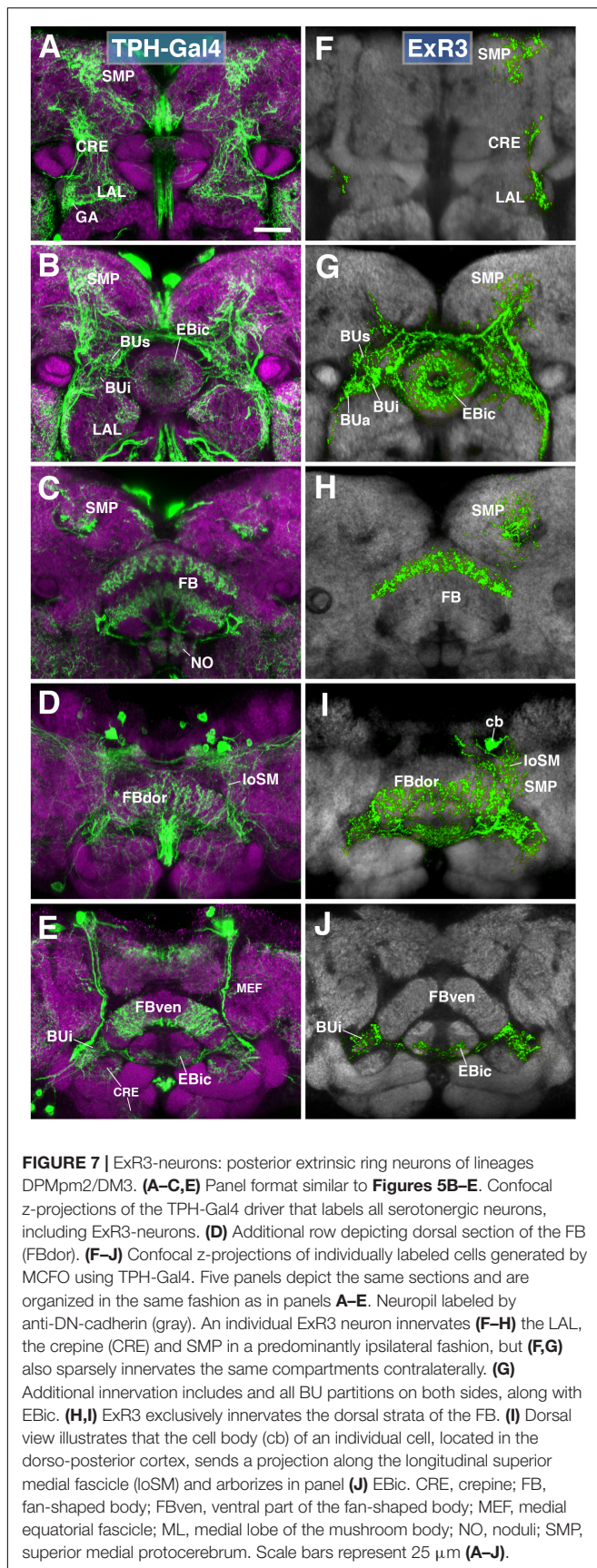


**Figure 6F**), but stay out of the GA and instead reach the medially adjacent CRE (**Figures 6E, F**). A third branch projects upward into a discrete subdomain of the SMP (**Figures 6F, G**).

- (3) A third type of PPM3 neuron (PPM3-LAL; not shown) does not innervate the EB or FB, but has bilateral projections to the lateral surface of the LAL. The second and third type of PPM3 neurons are not considered ExR-neurons due to their lack of EB innervation.

### ExR3

A subset of serotonergic neurons, visualized by the driver TPH-Gal4 (Park et al., 2006), also form part of the type II lineages, DM3-6. Labeled neurons have widespread projections throughout the protocerebrum, including the CX, BU, LAL, and CRE (**Figures 7A–E**). We generated MCFO single cell clones using the TPH-Gal4 driver (**Figures 7F–J**). Serotonergic neurons that innervate the EB, designated as ExR3, belong to the lineage DM3. Axons follow the loSM fiber system (**Figure 7I**). ExR3 neurons innervate EBic (**Figures 7G, J**), as well as a dorsal layer of the FB (**Figures 7H, I**). Additionally, they have bilateral projections to the BU (**Figures 7G, J**), and predominantly ipsilateral projection to the LAL, CRE, and SMP (**Figures 7F–I**).

### Anterior ExR-Neurons: Lineage BAMv1/LALv1

One additional subclass of ExR-neurons, designated as ExR4, was identified. Cell bodies of these neurons form a cluster in the anterior brain cortex, but, in contrast to DALv2 R-neurons, are located ventrally of the antennal lobe (**Figures 8A–D**). ExR4 neurons belong to the lineage BAMv1 (Lovick et al., 2013; Wong et al., 2013) – also called LALv1 (Ito et al., 2013; Yu et al., 2013), labeled by the driver 14G09-Gal4 (**Figure 8** and **Supplementary Movies 23, 24**). Axons of BAMv1 follow a highly characteristic pathway that initially leads posteriorly as part of the longitudinal ventromedial fascicle (loVM) and then makes a sharp turn dorsally (**Figures 8A, B**). The dorsal leg of the BAMv1 tract penetrates the LAL and gives off dense tufts of branches that fill the dorso-lateral quadrant of the LAL compartment (**Figures 8B, D**). Some branches reach forward into the GA of the LAL; others continue further dorsal into the CRE compartment (**Figures 8B, C**). Reaching the dorsal edge of the LAL, the axon tract of BAMv1 makes a second sharp turn, projecting medially toward the CX as the posterior part of the lateral ellipsoid fascicle (LEp; **Figure 8B**). Axons reach the CX at the cleft between the EB and FB, and from there project anteriorly into EBop (**Figures 8D, F**) and posteriorly toward the ventral strata (1–4, after Wolff et al., 2015) of the FB and into NO2 (**Figures 8E, F**). Denmark and syt.EGFP expression reveal that projections of BAMv1 neurons toward the EB and FB/NO are mainly axonal, with only a weak dendritic component; proximal arborizations in the LAL are preferentially dendritic (**Figures 8H, I**). Only the GA of the LAL has a significant axonal component (**Figure 8G**). This distribution of pre- and postsynaptic elements suggests that ExR-neurons of BAMv1 form a feed-back component connecting input and output domains within the CX circuitry: DALv2 ring neurons provide strong input to the EB, which is then transmitted

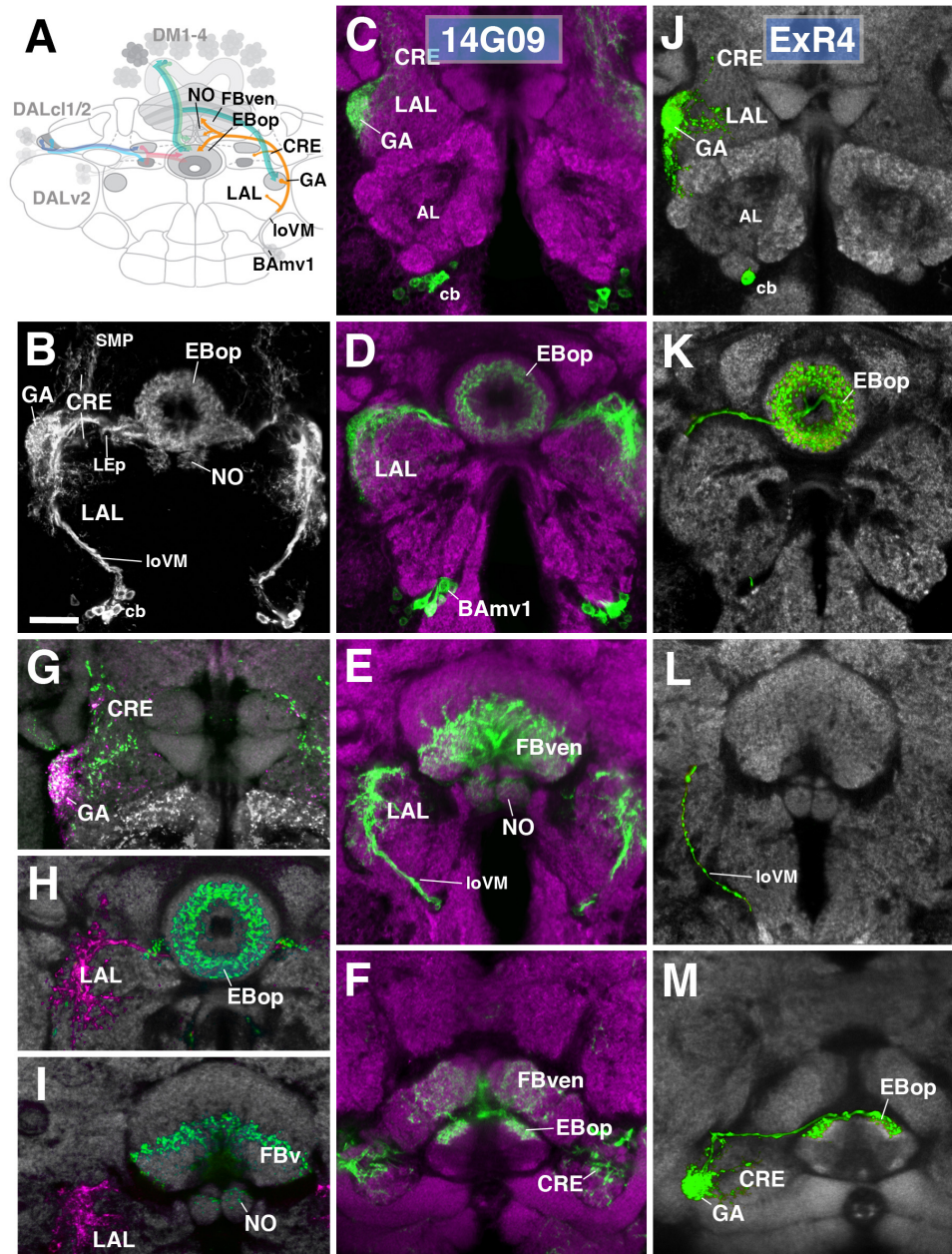


**FIGURE 8 |** Anterior ExR-neuron subclass of lineage BAmv1/LALv1. **(A)** Schematized overview of interacting neuronal populations of the EB from **Figure 1**, now including anterior ExR-neurons of lineage BAmv1 (orange). **(B)** Grayscale z-projection of ExR4, labeled by R14G09 > 10xUAS-mCD8::GFP. Z-projection spans from the gall (GA)/lateral accessory lobe (LAL) to the EB, and does not include the FB component of this driver (see below). Cell bodies (cb) of BAmv1 neurons send projections dorsally along the medial component of the ventral longitudinal fascicle (ioVM), which then extend from the GA/LAL to EBop. **(C–F)** Top three rows corresponds to frontal sections of R14G09 > 10xUAS-mCD8::GFP at three different antero-posterior depths (refer to **Supplementary Movie 23**). From top to bottom: **(C)** anterior section containing the GA/LAL, **(D)** intermediate section containing the EB and bulbs, **(E)** posterior section containing the FB and noduli (NO). Bottom row **(F)**; refer to **Supplementary Movie 24** is a horizontal section visualizing the length of the EB canal. R14G09-positive neurons are shown in green; neuropil is labeled with anti-DN-cadherin (magenta). **(G–I)** Corresponding sections in panels **C,D** using R14G09 labeled with the presynaptic marker syt.EGFP (green) and dendritic marker DenMark (red). Neuropil is labeled with anti-DN-cadherin (gray). **(J–M)** Confocal z-projections of individually labeled cells generated by MCFO using R14G09-Gal4. Four panels depict the same sections and are organized in the same fashion as in panels **C–F**. Neuropil labeled by anti-DN-cadherin (gray). An individual ExR4 neuron, with **(J)** its cell body (cb) located ventrally of the antennal lobe (AL), predominantly innervates the GA, with fine processes into the LAL, and **(K)** EBop. **(L)** ExR4 projects along the ioVM and does not innervate the FB. **(M)** Dorsal view illustrates the innervation in the GA and arborization in EBop. CRE, crepine; FBven, ventral region of the FB; LEp, posterior component of the lateral ellipsoid fascicle; SMP, superior medial protocerebrum. Scale bars represent 25 μm **(B–M)**.

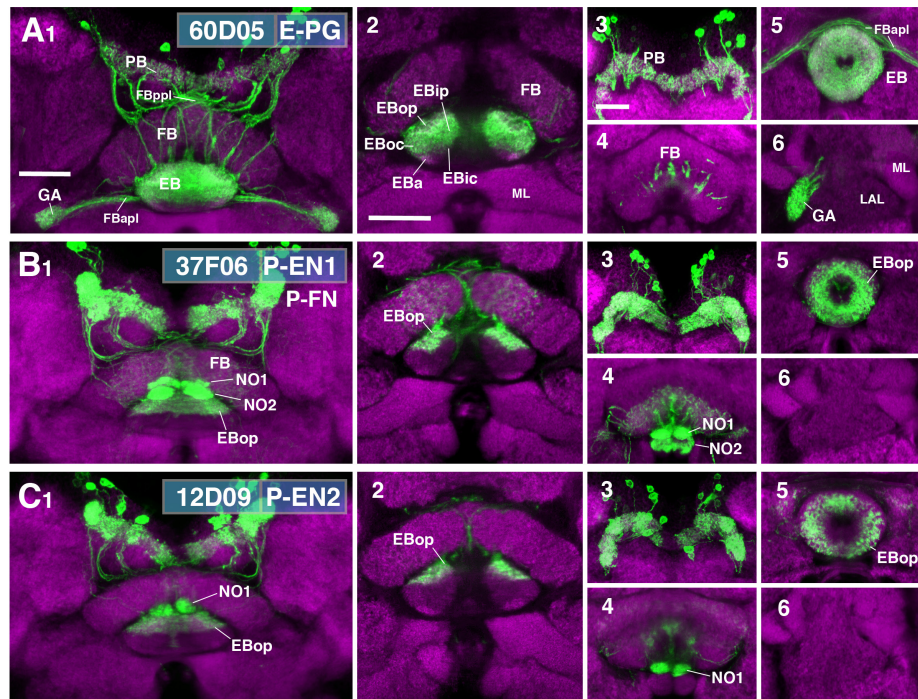


**FIGURE 9** | CX innervation patterns of Gal4 drivers labeling columnar neuron populations. **(A–C)** Confocal z-projections of Gal4 drivers that label columnar neuron classes. Each lettered, six-paneled module corresponds to an individual driver labeled with 10xUAS-mCD8::GFP (green); neuropil is labeled with anti-DN-cadherin (magenta). Left (1) is a z-projection from the dorsal view spanning the antero-posterior depth of the brain (anterior pointing downward). Second column (2) is a horizontal section visualizing the length of the EB canal; all five DN-cadherin positive domains are visible. Final two columns (3–6) are four frontal sections of the CX and its associated neuropils: (3) PB, (4) fan-shaped body (FB)/noduli (NO), (5) EB, (6) gall (GA)/lateral accessory lobe (LAL). Larger white annotations denote arborization-containing domains of interest; smaller white annotations represent spatial landmarks. **(A1–6)** R60D05-Gal4 (E-PG neurons). (2) EB innervation is diffuse throughout all EB domains (innervation appears restricted to the lateral region of EBa). **(B1–6)** R37F06-Gal4 (P-EN1). P-FN neurons are likely included. (2) EB innervation is restricted to outer posterior domain (EBop). **(C1–6)** R12D09-Gal4 (P-EN2). (2) EB innervation is restricted to outer posterior domain (EBop). FBapl and FBppl, anterior and posterior plexus of the fan-shaped body; ML, medial lobe of the mushroom body. Scale bars represent 25  $\mu\text{m}$  for panels **A1–C1**; 25  $\mu\text{m}$  for panels **A2–C2**; 20  $\mu\text{m}$  for panels **A3–6** to **C3–6**.

to the protocerebral bridge (PB) and the GA/LAL by columnar neurons. BAMv1 neurons form dendritic endings in the GA/LAL and feedback axons toward the EB.

We identified single cell MCFO clones of the BAMv1 lineage, corresponding to the ExR4 subclass (Figures 8J–M). Notably, these neurons have dense branches restricted to the GA and part of the anterior LAL surrounding the GA (Figure 8J) and to EBop (Figures 8K,M), but do not project to the posterior LAL, FB or NO (Figures 8K–M). This indicates that different neuron types of the BAMv1 lineage innervate the EB and the FB/NO, respectively.

## Columnar Neurons

While ring neurons terminate in the EB, further processing of sensory input requires synaptic partners that access other compartments of the CX. Several populations of columnar neurons fulfilling this requirement have been identified to date (Wolff et al., 2015; Wolff and Rubin, 2018). To investigate the spatial relationship of columnar neurons with ring neurons, we assessed Gal4 drivers previously shown to label distinct columnar neuronal populations (Seelig and Jayaraman, 2015; Wolff et al., 2015; Green et al., 2017; Turner-Evans et al.,

2017; Figure 9). These are populations of “wedge neurons” with arborizations in both peripheral and central parts of the EB, and two populations of “tile” neurons that project only to the peripheral EB. Shown in Figure 9A is one type of “wedge” neuron (PB<sub>G1–8</sub>.b.EBw.s-D/Vgall.b), also called E-PG neurons (Wolff et al., 2015; Turner-Evans et al., 2017), whose spiny (dendritic) terminal branches fill all EB domains except for part of EBa (Figures 9A1,2). Confirming previous descriptions, bulbous (axonal) endings are seen in the PB, as well as the GA (Figures 9A1,3,6).

Figures 9B,C show the projection patterns of P-EN neurons (PB<sub>G2–9</sub>.s.EBt.b.NO1.b; Wolff et al., 2015; Turner-Evans et al., 2017). This neuronal population has axonal endings in a tile-shaped domain, which we show here corresponds to EBop (Figures 9B2,5,C2,5). Outside the EB, projections are in the PB (Figures 9B3,C3) and the dorsal noduli (NO1; Figures 9B4,C4). Functionally, P-EN neurons fall into two subclasses, one (called P-EN1; Green et al., 2017; Turner-Evans et al., 2017) marked by the driver 37F06-Gal4 (Figure 9B), and the other one (P-EN2; Green et al., 2017) by 12D09-Gal4 (Figure 9C). In regard to terminal arborization in the EB, both lines appear identical (compare Figures 9B2,C2). However, 37F06-Gal4 is

likely expressed in an additional neuron type called PB<sub>G2-9.s-FBI3.b-NO<sub>2</sub>V.b</sub> (P-FN<sub>V</sub>; Wolff and Rubin, 2018), given labeling in the FB and NO2 (**Figure 9B4**).

## Mapping the Putative Postsynaptic Targets of R-Neurons

To identify downstream postsynaptic targets of distinct R-neuron subclasses, we utilized the anterograde *trans*-synaptic tracing method *trans*-Tango (Talay et al., 2017). In this approach, a bioengineered synthetic receptor system and downstream signaling components are expressed in a pan-neuronal fashion. Gal4-dependent expression of a presynaptically tethered cognate ligand leads to activation of the receptor specifically in postsynaptic neurons downstream of the Gal4 expressing population. Receptor activation then leads to proteolytic cleavage and release of the otherwise membrane-sequestered, orthogonal transcriptional activator QF. In this manner, the presynaptic neurons labeled by GFP under UAS control, can be visualized in conjunction with downstream targets, labeled by RFP under QUAS control. We applied *trans*-Tango to every R-neuron Gal4 driver to reveal, in principle, each output system in its entirety. However, in the absence of parallel methodology to demonstrate functional connectivity, we consider our findings to reveal “putative” targets, due to several potential caveats that merit consideration, some of which have been previously noted (Talay et al., 2017). In some cases, such as in R4d and R6, *trans*-Tango did not successfully yield RFP signal in the EB. This may be a consequence of insufficient expression levels of the synthetic ligand due to a weak Gal4 line, or a neural circuit that simply contains fewer synapses. Indeed, the Gal4 drivers that label R4d and R6 appear weaker, and are also some of the smallest populations in terms of cell number ( $8 \pm 0$  and  $2 \pm 0$  neurons PBH, respectively). However, a large or strongly Gal4-expressing GFP-positive population is not required to elicit a strong *trans*-Tango signal. We anecdotally observed strong RFP expression in other areas of the brain due to non-specific expression outside of the CX, even when the non-specific cells were sparse or weakly labeled. The strength of *trans*-Tango signal may also be determined by the neuron-specific expression level of the synthetic receptor, which cannot be assumed *a priori* to be uniformly expressed in every neuron throughout the brain, despite being under the control of a pan-neuronal promoter. This may result in sparse presynaptic labeling leading to strong postsynaptic labeling, or vice versa. This potential confound leads to the next consideration; a highly specific driver line is important to accurately interpret the postsynaptic signal. Given this, the specificity of each utilized driver can be visualized on the Janelia FlyLight website (see text footnote 1), and should be taken into account. Particularly for the CX, where neurons between neuropil compartments are recurrently connected, any non-specific neuronal labeling in another CX neuropil outside of the EB may yield a false positive signal for a ring neuron driver *trans*-Tango experiment. In a hypothetical example, it would be difficult to disambiguate whether RFP-positive neurons that interconnect the PB and EB are downstream of the ring neuron class of interest, or a non-specific neuron in the PB. Considering this, we opted

not to include *trans*-Tango results from R5 (58H05-Gal4); this driver line included additional neurons potentially innervating other CX neuropils (data not shown). Finally, the potential for false-positive signal due to reporter sensitivity or mislocalization of the overexpressed ligand, must always be considered (Talay et al., 2017). Despite the requirement for further validation, the *trans*-Tango results herein reveal heretofore unknown wiring principles of the R-neuron network. The findings of these experiments are summarized in **Figure 12**.

### R1

Neurons *trans*-synaptically labeled when using the R1 driver 31A12-Gal4 included R-neurons of the R1 and R3p subclass (**Figure 10A1**), as well as columnar E-PG and, likely, PB<sub>G2-9.s-FBI2.b-NO<sub>3</sub>A.b</sub> (P-FN<sub>A</sub>) neurons (Wolff et al., 2015; Wolff and Rubin, 2018). Thus, *trans*-Tango signal is detected in cell bodies of DALv2 neurons in the anterior cortex (**Figure 10A3**), as well as DM1-4 neurons in the posterior cortex (**Figure 10A2**). Many of these *trans*-synaptically labeled DALv2 neurons were also positive for GFP (**Figure 10A3**), indicating that R1 neurons form strong reciprocal connections among each other (homotypic interactions). In the EB neuropil, *trans*-Tango signal fills all compartments, but is enriched in EBip (**Figures 10A4,10**), which is targeted by R3p neurons (heterotypic interactions: interactions between neurons of one subclass and another). Accordingly, labeling is also detected in a subset of glomeruli within BUi (**Figure 10A5**), the dendritic compartment of R3p. *Trans*-Tango-positive projections of columnar neurons accounts for the labeling detected in the PB (**Figure 10A8**), outer EB domains (**Figures 10A4,10**), and GA (**Figure 10A11**). Signal ventrally of the GA (**Figure 10A11**), filling the lateral surface of the LAL, is attributable to the reciprocally connected R1 neurons (**Figures 10A5-7,11**). In addition to E-PG neurons, the *trans*-Tango-positive columnar neurons also appeared to include P-FN<sub>A</sub> neurons, based on signal detectable in the FB and ventral noduli (Wolff et al., 2015; Wolff and Rubin, 2018; **Figure 10A9**). The responsible connection between R1 and P-FN<sub>A</sub> neurons to which this label could be attributable, could be a sparse, posteriorly projecting neurite of R1-neurons to the FB which was periodically observed (data not shown).

### R2

Cells identifiable as targets of R2-neurons include other ring neurons of the R4d, R3d, and R2 subclasses, in addition to columnar E-PG neurons. In the anterior cortex, GFP and *trans*-Tango label overlaps weakly, and perhaps in only a small proportion of cell bodies (**Figure 10B3**), indicating that reciprocal connections among R2-neurons are present but not very pronounced. The EB neuropil is ubiquitously filled with *trans*-synaptic label, but shows enriched signal in EBic, which is targeted by R3d, and the peripheral fringe of EBoc, innervated by R4d (**Figure 10B4**), suggesting prominent heterotypic interactions. In accordance with the notion that R3d and R4d are postsynaptic partners of R2, we find *trans*-Tango labeling in a posterior-lateral part of BUs (**Figure 10B5**), shown above to be dendritically innervated by R4d (see **Figures 3A3,4**),

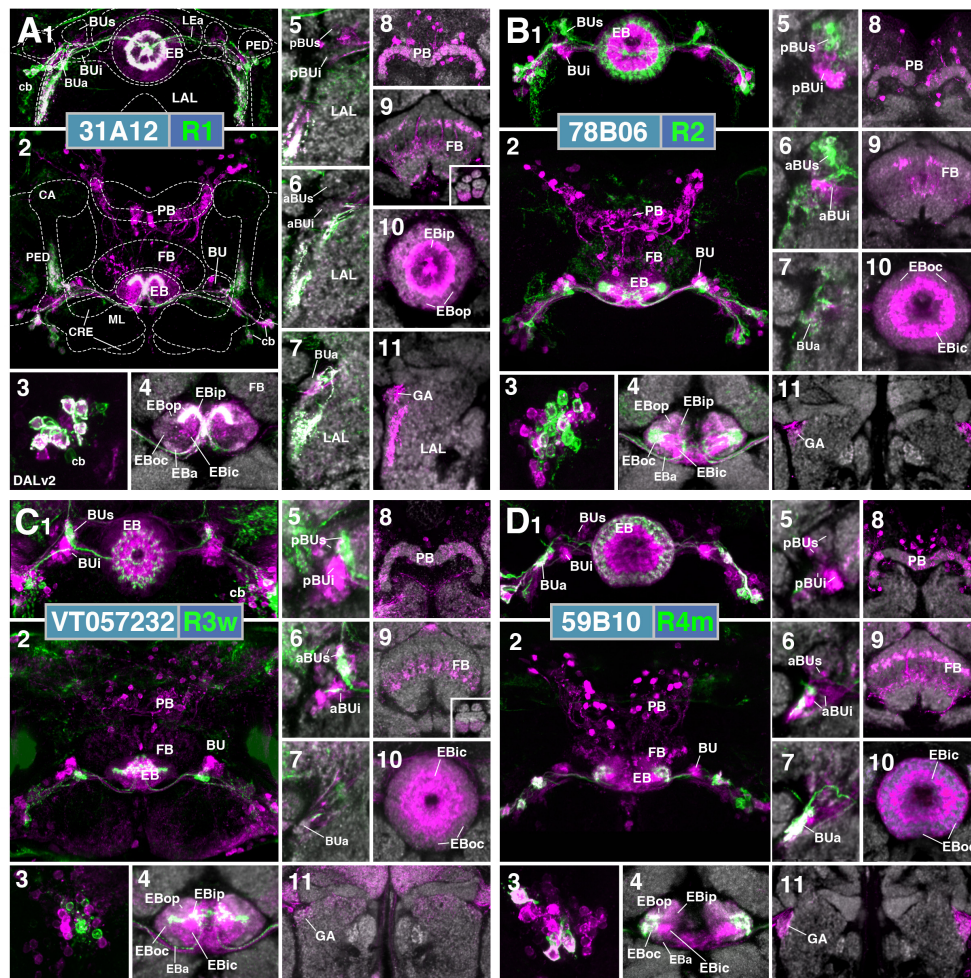


**FIGURE 10 |** Putative postsynaptic partners of R-neurons revealed by *trans*-Tango. **(A–D)** Confocal z-projections of Gal4 drivers that label distinct R-neuron subclasses in conjunction with *trans*-Tango mediated labeling of postsynaptic neurons. Each lettered, 11-paneled module corresponds to an individual driver. Gal4-expressing R-neurons labeled by GFP under UAS control (green) and putative postsynaptic neurons are labeled by RFP under *trans*-Tango mediated QUAS control (magenta). Larger white annotations denote arborization-containing domains of interest; smaller white annotations represent spatial landmarks. Module organization outlined below: (1) Frontal z-projection spanning from R-neuron cell bodies to the ellipsoid body (EB)/bulbs (BU). (2) Z-projection from the dorsal view spanning the antero-posterior depth of the brain (anterior pointing downward). (3) Image of DALv2 R-neuron cell bodies (cb) to illustrate degree of colocalization between pre- and post-synaptic neurons, an indication of homotypic interactions within a cell type. (4–11) Neuropil is labeled with anti-DN-cadherin (gray). (4) Horizontal section of the EB spanning the length of the EB canal. (5–7) Frontal sections of the bulb at three different depths. From top to bottom: (5) posterior section containing the posterior regions of the superior (pBUs) and inferior (pBUi) bulb, (6) intermediate section containing the anterior regions of the superior (aBUs) and inferior (aBUi) bulb, (7) anterior section containing the anterior (BUa) bulb. (8–11) Isolated postsynaptic targets (shown in magenta) throughout the CX (Gal4-expressing neurons are shown not shown). Four frontal sections of the CX and its associated neuropils; from top (posterior-most) to bottom (anterior-most): (8) PB, (9) FB and noduli (NO) in inset when applicable, (10) EB, (11) gall (GA)/lateral accessory lobe (LAL). **(A1–11)** (R1) R31A12-Gal4 > *trans*-Tango. **(B1–11)** (R2) R78B06-Gal4 > *trans*-Tango. **(C1–11)** (R3w) VT057232-Gal4 > *trans*-Tango. **(D1–11)** (R4m) R59B10-Gal4 > *trans*-Tango. CRE, crepine; ML, PED, and CA, medial lobe, peduncle, and calyx of the mushroom body, respectively; LEa, anterior component of the lateral ellipsoid fascicle.

and in the posterior region of the inferior bulb (pBUi), corresponding to R3d (Figure 10B5). Labeling of cell bodies in the posterior cortex, occupied by DM1–4 (Figure 10B2), and of neuropil including the PB (Figure 10B8), outer EB (Figure 10B10) and GA (Figure 10B11) is attributable to E-PG neurons targeted by R2. Sparse label in the FB corresponds to the through-going fibers of columnar E-PG neurons, in addition to other neuronal populations of unclear identity (Figure 10B9).

### R3w

The R3w subclass could be viewed as an intermediary between outer and inner R-neurons in terms of the projection of proximal branches (ventral part of BUs) and distal branches (narrow EBic domain, reaching into EBoc). Correspondingly, R3w neurons, like outer subclasses R2 and R4m, target a good number of columnar E-PG neurons (Figures 10C2,8,11), in addition to a small number of R2 neurons (sparse RFP label in EBoc and BUs; Figures 10C4–6). Strongest RFP signal is seen in the inner EB

domains and BU<sub>i</sub>, indicating R3d, and particularly R3p, as major targets (**Figures 10C4–6,10**). Based on the sparse innervation in aBU<sub>i</sub>, R3m could also be a potential target (**Figure 10C6**). It should be noted that the driver VT057232-Gal4, which is used here to label R3w, is also expressed in numerous additional neurons throughout the brain, which may account for some of the RFP signal (**Figure 10C2**). For example, staining of the ventral noduli (NO3; **Figure 10C9**, inset), presumably corresponding to one of the P-FN populations, is unlikely to be attributable to R3w R-neurons as presynaptic partners.

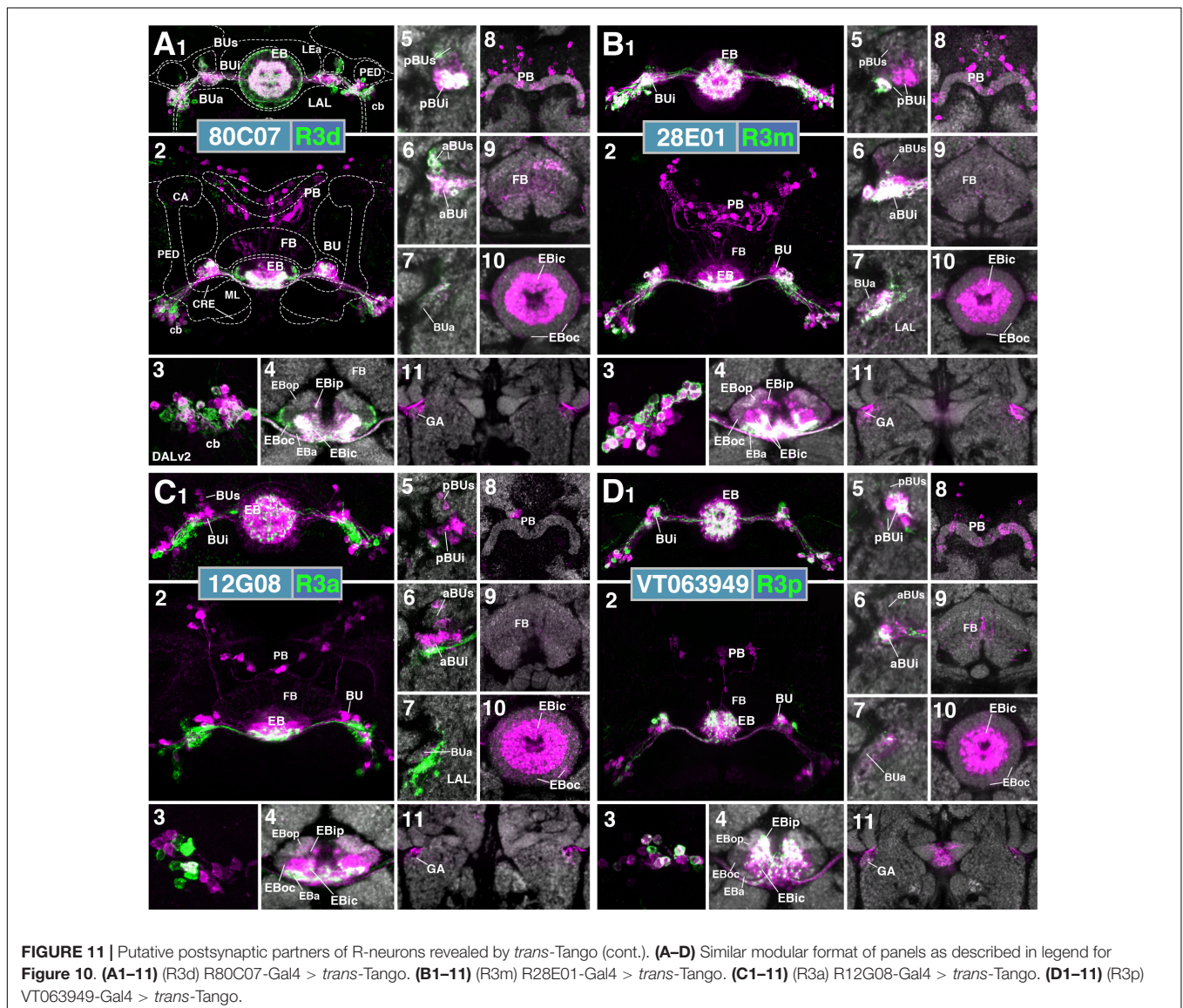
### R4m

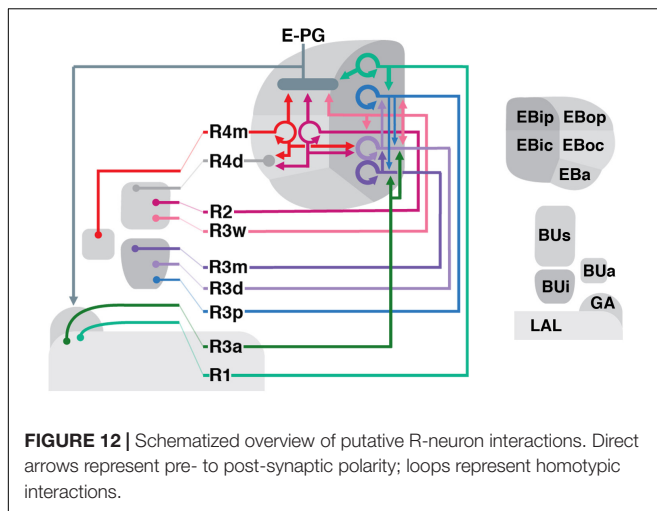
R4m neurons innervate EBoc, similar to R2, but have their dendritic projection toward BU<sub>a</sub>. Using the R4m driver line 59B10-Gal4, we see *trans*-synaptic label of R-neuron subclasses R4m, R4d, and R3d, as well as a large fraction of columnar E-PG neurons (**Figure 10D**). Signal is concentrated in EBic (R3d) and

periphery of EBoc (R4d) (**Figures 10D4,10**). In the BU, *trans*-synaptic label covers BU<sub>a</sub>, corroborating reciprocal interactions among R4m (**Figure 10D7**), in addition to the lateral part of BUs (R4d; **Figure 10D5**) and pBU<sub>i</sub> (R3d; **Figure 10D5**). There is a large number of RFP-positive DM1–4 columnar neurons in the posterior cortex (**Figure 10D2**), projecting dense arrays of fiber tracts that innervate the PB (**Figure 10D8**), through the FB (**Figure 10D9**), to the EB and GA (**Figures 10D10,11**).

### R3d/4d

The driver line 80C07-Gal4 marks R3d neurons with axonal projections to EBic and dendritic innervation of pBU<sub>i</sub>. This pattern is confirmed when using the line in the context of *trans*-synaptic labeling (**Figures 11A1,5**). However, likely as a consequence of enhancement of GFP signal with the use of anti-GFP antibody, we also saw GFP signal in the peripheral fringe of EBoc and the lateral part of BUs, indicating that 80C07-Gal4 is





also expressed in R4d neurons. It is therefore difficult to assign the observed *trans*-synaptic label induced by this line to either one of these populations. We observe *trans*-synaptic label in both R-neurons in the anterior cortex, and DM1–4 columnar neurons in the posterior cortex (Figures 11A1,2). Approximately half of 80C07-expressing R-neurons are also labeled *trans*-synaptically, suggesting strong reciprocal connectivity among R3d and/or R4d (Figure 11A3). In the EB neuropil, *trans*-Tango signal is highly concentrated in EBic and EBip, and the peripheral fringe of EBoc (Figures 11A4,10). This pattern again argues for strong reciprocal interactions of R3d and R4d, as well as contacts between R3d and R3p. *Trans*-synaptic label in the BU also largely overlaps with GFP signal in pBUi and lateral part of BUs (Figures 11A5,6), that are dendritically innervated by R3d and R4d neurons, respectively. Exclusive label of glomeruli in the dorsal part of BUi (Figure 11A5) corresponds to R3p which targets this region (see Figure 2F). *Trans*-synaptic labeling of columnar neurons is sparse, with only few cell bodies in the posterior cortex (Figures 11A2,8), and faint/restricted labeling of the outer EB domains and the GA (Figures 11A10,11). The identity of *trans*-synaptically labeled neurons spottily innervating the FB (Figure 11A9) is not clear.

### R3m

The pattern of *trans*-synaptically labeled neurons by the R3m driver 28E01-Gal4 largely resembles that described previously for R3d. R3m neurons have strong reciprocal interactions, with the majority of their cell bodies being positive for both GFP and RFP (Figures 11B1,3). Based on the *trans*-synaptic labeling observed in EBic as well as, weakly in EBip and the periphery of EBoc (Figure 11B4), R3d, and perhaps R3p and R4d neurons are also targeted by R3m. This is corroborated by labeling in the BU (Figures 11B5,6), which includes pBUi (R3d), dorsal part of pBUi (R3p), and weakly, the lateral part of BUs (R4d). *Trans*-synaptic labeling of E-PG neurons is sparse (Figures 11B8,11).

### R3a

Whereas the inner R-neuron subclasses R3d, R3m and R3p preferentially form homotypic connections among each other,

the R3a subclass targets EBic in a heterotypic manner. Thus, there is but little overlap of GFP and RFP in R3a neuronal somata (Figures 11C1–3). Strong target label is seen in EBic (Figures 11C4,10) and throughout BUi (Figures 11C5,6), indicating inner R-neuron subclasses R3d and R3m as preferred targets of R3a. Sparse label in EBoc and BUs suggests that some R2 neurons might also be among the R3a targets (Figures 11C4–6,10). Furthermore, a very small number of E-PG neurons, and a matching faint RFP signal in EBop and EBoc, as well as the GA, appear to be targeted by R3a (Figures 11C2,4,11).

### R3p

R3p resembles R3d and R3m in forming strong homotypic interactions, as seen from overlapping GFP and RFP signal in cell bodies (Figures 11D1,3), EBip (Figures 11D1,2,4) and dorsal part of pBUi (Figure 11D5). In addition, based on extensive RFP signal throughout BUi (Figures 11D5,6), R3p targets other subclasses of inner R-neurons, notably R3d and R3m. We observed only small numbers of RFP-positive E-PG neuronal cell bodies (Figure 11D2,8), matching only faint label of PB, outer EB, and GA (Figure 11D4,8,10,11).

## DISCUSSION

This work serves to build upon previous anatomical studies by further clarifying the neuronal architecture of the *Drosophila* EB. Five definitive DN-cadherin domains constituting the EB neuropil provide fiducial landmarks with which neuron classes can be placed into spatial context. Based on this framework, we report several novel ring neuron subclasses and propose potential interactions between ring, columnar, and neuromodulatory neurons in the EB. Lastly, we experimentally mapped putative postsynaptic partners of R-neurons using *trans*-Tango, revealing insight into how information may be distributed throughout the EB and the rest of the CX. In addition to the neuroanatomical description of different populations, the identification of driver lines enables genetic access to label or manipulate these populations. This provides an entry point for future studies to probe the functional properties of each class and test the interactions proposed herein. In the following, we summarize the primary findings, speculate on the functional significance of CX wiring principles, and place our study into a developmental-neuroanatomical context with previous works in *Drosophila* and homologous structures in other insects.

### Information Flow in the EB Network: Input, Recurrence, Output, and Neuromodulation

The CX is viewed as a critical hub for goal-directed navigational behavior in insects. Streams of sensory information from different modalities must converge onto this center of sensorimotor integration to guide navigational decisions based on current trajectory, learned information, and motivational state (Heinze, 2017). Central to this notion was the identification of a stable compass representation that tracks the flies heading in the E-PG neuron population. The robustness of this neural

correlate of angular orientation, manifested as a single calcium activity “bump” that moves around the EB, depends on both visual and proprioceptive cues (Seelig and Jayaraman, 2015). Heavily relying upon studies in other insect species as a basis for comparison (el Jundi et al., 2014), recent progress has been made toward identifying the neural pathways that transmit sensory information to the *Drosophila* CX, with visual input being the most well characterized. The fly CX receives visual information via the anterior visual pathway (AVP), a circuit defined by three successive layers. Information is transmitted from the optic lobe medulla to the anterior optic tubercle, from the tubercle to the bulb (BU), and from there to the EB, via medullo-tubercular (MeTu), tuberculo-bulbar (TuBu), and DALv2 ring neurons (R-neurons), respectively (Omoto et al., 2017). Parallel ensembles of TuBu neurons terminate in a topographically organized fashion onto the microglomerular dendrites of distinct R-neuron subclasses within the BU (Omoto et al., 2017). Specific computations are implemented across successive layers in this pathway, such as the integration of recent visual history and self-motion, which may inform downstream behavior (Shiozaki and Kazama, 2017; Sun et al., 2017). Ring neurons transmit processed visual information concerning features and landmarks to the EB, likely as a stable allothetic reference to guide bump dynamics in E-PG neurons (proposed in Seelig and Jayaraman, 2015; Turner-Evans et al., 2017). The interaction between tangential elements of the EB and columnar neurons such as E-PG neurons has been suggested in other insects (el Jundi et al., 2014), and confirmed by GFP reconstitution across synaptic partners (GRASP) in *Drosophila* (Xie et al., 2017). Indeed, we provide further evidence via *trans*-Tango that R2 neurons, which are tuned to visual features (Seelig and Jayaraman, 2013), provides direct presynaptic input to E-PG neurons (Figure 10B, 12). The calcium activity bump in E-PG neurons also shift in total darkness, demonstrating the existence of a proprioceptive input channel that can update the heading representation in the EB in the absence of visual input. We posit that transmission of idiotropic cues to the CX is mediated in part by R1 and/or ExR4 neurons, as their neurite distribution and polarity suggests feedback from the LAL, a proposed motor signaling center (Figures 2, 8 and Supplementary Figure 2) (Namiki and Kanzaki, 2016).

Conceivably, the information received by different R-neuron subclasses is transmitted to their ring-shaped neurites, and is processed via connections within the same subclass (homotypic interactions) and/or between subclasses (heterotypic interactions), the extent of which depends on the R-neuron subclass in question (Figures 10–12). As such, the R-neuron system likely displays recurrent connectivity to enable persistent activity required for memory processes, as has been shown for mushroom body circuits that support courtship memory (Zhao et al., 2018). Indeed, inner ring neurons (likely R3d and R3p), which comprise a critical nucleus of visual working memory (Neuser et al., 2008; Rieche et al., 2018), display prominent homotypic interactions (Figures 11A,D, 12). Future work to define the mechanisms underlying intra-subclass interactions and experiments to perturb them, are required to assess the functional significance of these homotypic interactions.

R-neurons, particularly subclasses of which occupy peripheral EB domains, provide input to several different columnar neuron populations. To our knowledge, this study provides novel insight into the nature of subclass-specific, input–output communication between the ring and columnar networks. An important avenue of future work will be to elucidate the tuning properties of each R-neuron subclass and determine the contribution of each input to compass representation. Presumably, R-neuron subclasses that provide prominent, direct input to E-PG neurons, such as R2 or R4m (Figure 12), would exhibit the most influence over compass representation.

Circuit flexibility is likely facilitated by neuromodulatory input on a moment-by-moment basis, which may reconfigure information flow through the network and thus the output of the system. Neuromodulation would likely occur at multiple processing stages, as evidenced by the wide-spread neurites of dopaminergic neurons. For example, a single PPM3 neuron, innervates the GA/LAL, BU, and EBoc/op. We envisage that neurite-specific signaling and plasticity may regulate distinct processing nodes, akin to what has been demonstrated for dopaminergic neurons that encode protein hunger (Liu et al., 2017). Similarly, 5-HT may also influence R-neuron activity as projections from the serotonergic neurons, ExR3 [corresponding to the posterior medial protocerebrum, dorsal cluster (PMPD; Pooryasin and Fiala, 2015)], most prominently innervate EBic (Figures 7E,G,J). The effect of serotonin may be receptor and circuit specific; distinct 5-HT receptor isoforms are differentially expressed in specific R-neuron subclasses (Gnerer et al., 2015).

### Three-Dimensional Architecture of the EB

For clarity, the five EB domains defined by the global marker DN-cadherin should be reconciled with previously used anatomical terminology of the EB (Omoto et al., 2017; Figure 1). Frontal sections of the EB at different anteroposterior depths shows that DN-cadherin domains are distinct, annular entities. These domains correspond to “layers” in other insects, and have sometimes been also referred to as layers in *Drosophila* as well (Young and Armstrong, 2010b). Therefore, N-cadherin EB domains are synonymous with layers. Each domain is best represented using a “dorsal standard view”: a horizontal section through the EB containing a lengthwise perspective of the EB canal (Figure 1). From this standard view, the N-cadherin domains are also clearly organized along the anteroposterior axis. Three anteroposterior subdivisions of the EB have been referred to as “shells,” in line with terminology used for the FB (Wolff et al., 2015). We propose that the anterior most shell encapsulates the anterior domain of the EB (EBa), and therefore consists of only one layer. The intermediate shell (called medial shell in Wolff et al., 2015) encapsulates the inner central (EBic) and outer central (EBoc) domains, and consists of two layers. Finally, the posterior shell encapsulates the inner posterior (EBip) and outer posterior (EBop) domains, and consists of two layers. For example, P-EN neurons occupy the EBop domain, which resides in the posterior EB shell (Figures 9B,C).

Lin et al. (2013) defined four substructures denoted as “rings” [EB<sub>A</sub> (Anterior), EB<sub>O</sub> (Outer), EB<sub>C</sub> (Center), EB<sub>P</sub> (Posterior)], which were based on anti-disks large (DLG) immunostaining and roughly correspond to the DN-cadherin domains. Like the DN-cadherin domains, each “ring” was proposed to contain specific R-neuron subclasses. Based on the ring neuron subclasses proposed by Lin et al. (2013) to comprise each “ring” (see below), we infer that EB<sub>A</sub> from Lin et al. (2013) corresponds to EB<sub>A</sub> and EB<sub>C</sub> in our classification system. Furthermore, EB<sub>O</sub> is EB<sub>O</sub>, EB<sub>C</sub> is EB<sub>IP</sub>, and EB<sub>P</sub> is EB<sub>OP</sub>.

How does the annular domain structure of the *Drosophila* EB compare to the lower division of the central body (CBL) described for other insects? Similar to the EB, the CBL represents a multilayered neuropil compartment formed by the neurite contributions of tangential and columnar elements. In insects such as locust (*Schistocerca gregaria*), which will be used as the primary basis for comparison in the following, the kidney bean or sausage-shaped CBL corresponds to the torus-shaped EB in *Drosophila* (Ito et al., 2014; Pfeiffer and Homberg, 2014). In locusts, the CBL is effectively located ventrally of the upper division of the central body (CBU), whereas the homologous structures in *Drosophila* (EB and FB, respectively) are arranged in an antero-posterior fashion. This difference is reflective of a 60° anterior tilt of the locust neuraxis, as evidenced by the peduncle, which extends horizontally in flies but is oriented almost vertically in the locust (von Hadeln et al., 2018). In the dung beetle (*Scarabaeus lamarcki*) and monarch butterfly (*Danaus plexippus*), the CBL are also sausage-shaped, but the neuraxis orientation is like that of *Drosophila* (Heinze and Reppert, 2012; Immonen et al., 2017). Differences in neuraxis orientation influence the comparison between the internal architecture of the locust CBL and fly EB. The locust CBL is subdivided along the dorso-ventral axis into six horizontal layers (although not stacked seamlessly on top of one another). Based on the expression of global markers, the *Drosophila* EB is divided into toroidal domains (EB<sub>A</sub>/ic/oc/ip/op; **Figure 1**). Considering the tilt in neuraxis, we posit that dorsal strata (layers 1–2) of the locust CBL roughly correspond to more posterior domains (EB<sub>IP</sub>/op) of the fly EB, whereas ventral strata (layers 3–6) correspond to more anterior EB domains (EB<sub>A</sub>/ic/oc). Corroborating this notion is the fact that fly P-EN neurons innervate EB<sub>OP</sub>, and the locust homologs (called CL2 neurons) innervate dorsal layers of the CBL (Müller et al., 1997).

## Lineage-Based Architecture of the EB

The EB and its domains, as well as other structures of the CX, are established by the neurite contributions of distinct neuronal populations. How is the neuronal diversity and connectivity of the CX developmentally established? The CX, and brain in general, is organized into structural-genetic modules called lineages; a lineage comprises the set of sibling neurons derived from an individual neural progenitor (neuroblasts). Each neuroblast forms a spatially discrete cluster of neurons with shared wiring properties; sibling neurons extend a limited number of fasciculated axon tract(s) and innervate specific brain compartments. Most brain lineages are “type I” neuroblast lineages, whose neuroblasts undergo a series of asymmetric

divisions each of which renews the neuroblast and produces a ganglion mother cell. Columnar neurons of the CX are generated from four type II lineages which are larger and more complex than type I, with neuroblasts first producing a set of intermediate progenitors which in turn, give rise to ganglion mother cells (Bello et al., 2008; Boone and Doe, 2008; Bowman et al., 2008; Wang et al., 2014; Doe, 2017).

While the columnar neurons contributing to the EB are derived from type II lineages, the tangential elements (R-neurons) are largely derived from a single paired type I neuroblast, forming the lineage DALv2 (also called EBa1) (Ito et al., 2013; Wong et al., 2013; Yu et al., 2013; Omoto et al., 2017). Neurons of the DALv2 lineage have been studied in developmental contexts in a number of previous works (Kumar et al., 2009; Larsen et al., 2009; Spindler and Hartenstein, 2011; Lovick et al., 2017; Minocha et al., 2017; Xie et al., 2017). Production of secondary neurons by DALv2 begin around 24 h after hatching (Lovick and Hartenstein, 2015). According to Kumar et al. (2009), one of the DALv2 hemilineages undergoes apoptotic cell death, implying that the DALv2 R-neurons forming the adult EB represent a single hemilineage. Cursory heat-shock inducible single-cell clonal analysis carried out in the present study suggests that distinct R-neuron subclasses are born during specific time windows and therefore represent sublineages of DALv2 (**Figure 4**). Thus, clonal induction shortly after the onset of secondary neuroblast proliferation (20–48 h after hatching) yielded exclusively outer R-neurons of the R4m subclass. At increasingly later time points, these types of clones become rare, and disappeared entirely at induction times after 96 h. The converse is the case for inner ring neurons (R3d/m), which could be induced in increasing numbers with later time points of induction. Given that only a fraction of the overall number of R-neuron subclasses was represented among our clones, additional studies are required to settle the exact birth order of different R-neuron subclasses.

## Ontology of the Ring Neuron Classification System

In the following, we provide a brief historical account of ring neuron definitions, attempt to resolve discrepancies in the literature when possible, and provide rationale for naming conventions used in this work.

Based on the description by Hanesch et al. (1989), the R-neuron type corresponds to ring neurons of the DALv2 lineage, with four R-neuron subclasses described in this initial study (R1–4). Two other ring neuron types were designated as “extrinsic ring neurons” (ExR-neurons), based on large projections outside of the EB; in this study, we pool neurons with this feature into a single type, the ExR-neurons. The first type of extrinsic R-neuron (the ExR1 subclass) described in Hanesch et al. (1989) likely corresponds to helicon cells. The second type (the ExR2 subclass) was not fully reconstructed by Hanesch et al. (1989), but due to its innervation of the caudal EB, ExR2 may correspond to the EB<sub>OP</sub>-innervating PPM3 dopaminergic neuron (**Figures 6E–H**), and thus our rationale for this designation. The serotonergic neurons that innervate the EB, corresponding to the PMPD neurons, we designate as ExR3. Therefore, ExR1–3 are posteriorly

localized ExR-neurons, likely deriving from the DM3–6 lineages. Due to its wide arborization and non-DALv2 based origin, we designate ring neurons of lineage BAmv1, with perikarya in the anterior cortex, as a fourth type of ExR-neuron (ExR4); we cannot exclude the possibility that ExR2 from Hanesch et al. (1989) may correspond to ExR4-neurons, as they too innervate the caudal EB. Furthermore, the “P”-neurons, described in Lin et al. (2013) as having ventrally localized cell bodies and also innervate the caudal EB, likely correspond to what we designate as ExR4-neurons.

Renn et al. (1999) was the first to conduct a genetic analysis of the EB neuropil, using enhancer-trap technology. Renn et al. (1999) described driver line c105 to label R1 neurons (**Supplementary Figure 1A**), due to their centrifugal arborization pattern, inner ring localization, and extension into the posterior layers of the EB, a similar description to that of Hanesch et al. (1989). However, c105-positive R1 neurons exhibit ventrally projecting neurites into the LAL and lack BU microglomeruli (Renn et al., 1999; **Supplementary Figures 1A3–5**), in contrast to what was defined as R1 in Hanesch et al. (1989). Therefore, we speculate that Renn et al. (1999) identified a novel R-neuron class, distinct from R1 as described by Hanesch et al. (1989). However, due to R1 being the predominant designation this R-neuron subclass thereafter (Renn et al., 1999; Young and Armstrong, 2010b; Lin et al., 2013), we retain this classification in our study.

If R1 from Renn et al. (1999) was a previously undescribed class, what was R1 from Hanesch et al. (1989)? Based on the camera lucida drawn Golgi stained preparations and the description of R1 being “restricted to the inner zone lining the EB canal” we propose that R1 from Hanesch et al. (1989) was interpreted by Renn et al. (1999) as R3. Henceforth, the predominant description of R3, which has been heavily investigated for their role in visual working memory, is that of “inner ring” R-neurons, a convention we also therefore retain (Neuser et al., 2008; Young and Armstrong, 2010b; Kuntz et al., 2012; Lin et al., 2013; Omoto et al., 2017). However, it is unclear which of the several R3-neuron subclasses with BU microglomeruli identified in this study (R3m, R3d, R3p), correspond to R1 described in Hanesch et al. (1989).

Presuming R1 being renamed R3 by later authors, which R-neuron subclass corresponds to R3 in Hanesch et al. (1989)? R3 was shown to have a centrifugal innervation pattern, restricted to the rostral half of the EB, and importantly, exhibited branches with terminals in the inner and outer ring (Hanesch et al., 1989). To our knowledge, this R-neuron subclass has not been described in any study thereafter, and likely corresponds to R3w of the present study (**Figure 2G**).

R4 was described by Hanesch et al. (1989) to project in a centripetal fashion and extend terminals into the outermost zone. Renn et al. (1999), noted two neuron subclasses that exhibit these features, and referred to these “R4-type” neurons as R4m and R4d. The camera lucida drawing of R4 in Hanesch et al. (1989) displays a ventrally localized microglomerulus (likely corresponding to BUa), a description that matches that of R4m in subsequent studies (Renn et al., 1999); we postulate that R4d was a class that exhibited R4-like wiring properties, newly identified by Renn et al. (1999) altogether.

R2 in former studies [Hanesch et al., 1989; labeled by c42 (**Supplementary Figure 1B**; Renn et al., 1999) and EB1-Gal4 (**Supplementary Figure 1C**; Young and Armstrong, 2010b)] has axons within the EBoc domain, along with R4m (**Figures 3B5,6**). In a more recent paper (Lin et al., 2013), the designation “R2” became associated with neurons projecting to the “anterior ring” (synonymous with EBa from this study). The designation of these anterior EB R-neurons as “R2” has carried forward to other studies, when their critical role in the regulation of sleep homeostasis was identified (Liu et al., 2016; Donlea et al., 2018). It should be noted that Liu et al. (2016) documented the distinction between what had historically been referred to as R2, and what had been referred to as “R2” in Lin et al. (2013). “R2” in Lin et al. (2013) appears morphologically similar to a subclass revealed by the 52y driver in Young and Armstrong (2010b), which were not given a specific name. We used the name R5 for these anterior R-neurons (Omoto et al., 2017) and propose to retain this designation to prevent future studies from equating them with what has been historically referred to as R2.

In more recent studies, the driver 38H02-Gal4 has been described as labeling R4 (or an R4-subset), in several studies (Ofstad et al., 2011; Dus et al., 2013; Park et al., 2016). 38H02-Gal4 does in fact label R4m (based on BUa microglomeruli and centripetal EBoc innervation pattern), but also strongly labels R5 (**Supplementary Figure 1J**). Two other drivers, 15B07-Gal4 and 28D01-Gal4, were used to target EB neurons required for visual-thermal associations in place learning (Ofstad et al., 2011), and were described as labeling “R1 and R4,” or “R1 alone,” respectively. Anatomical re-assessment of these drivers reveals that 15B07-Gal4 labels R3d, R3p, and R4d (**Supplementary Figure 1I**), whereas 28D01-Gal4 labels a neuron subclass indicative of R3m (**Supplementary Figure 1D**).

In summary, the dorsal view of the EB in conjunction with DN-cadherin immunostaining provide criteria to more definitively identify ring neuron subclasses for future studies. The model organism *Drosophila* offers unique advantages to examine the circuit motifs that support the broadly relevant computations underlying the processes attributed to the CX; (1) the neurons comprising the CX are spatially and numerically confined, (2) genetic access to label, assess connectivity between, or functionally manipulate, specific neuron types within it, and (3) amenability to electro- or optophysiological recordings, oftentimes in the behaving animal. To fully leverage these advantages, we provide a systematic description of the ring neuron subclasses comprising the EB, genetic tools to access them, and provide insight into their interactions with other neurons of the CX (Omoto et al., 2018).

## AUTHOR CONTRIBUTIONS

JO contributed in conceptualization. JO and B-CN contributed in methodology. JO, B-CN, PK, and JL contributed in investigation. JO and VH contributed to writing the original draft. JO, B-CN, PK, JD, and VH contributed to writing the review and editing. JO, B-CN, PK, and VH contributed in visualization. JD and VH supervised and acquired the funding.

## FUNDING

This work was supported by the NIH (Grants R01 NS096290 to VH and R01NS105967 to JD), additional support provided by the University of California, Los Angeles Dissertation Year Fellowship and the A.P. Giannini Postdoctoral Fellowship (to JO).

## ACKNOWLEDGMENTS

We thank the Bloomington Stock Center and the Developmental Studies Hybridoma Bank for fly strains and antibodies. We also thank the following labs for kindly providing fly lines:

## REFERENCES

- Bayraktar, O. A., and Doe, C. Q. (2013). Combinatorial temporal patterning in progenitors expands neural diversity. *Nature* 498, 449–455. doi: 10.1038/nature12266
- Bello, B. C., Izergina, N., Caussinus, E., and Reichert, H. (2008). Amplification of neural stem cell proliferation by intermediate progenitor cells in *Drosophila* brain development. *Neural Dev.* 3:5. doi: 10.1186/1749-8104-3-5
- Bender, J. A., Pollack, A. J., and Ritzmann, R. E. (2010). Neural activity in the central complex of the insect brain is linked to locomotor changes. *Curr. Biol.* 20, 921–926. doi: 10.1016/j.cub.2010.03.054
- Boll, W., and Noll, M. (2002). The *Drosophila* pox neuro gene: control of male courtship behavior and fertility as revealed by a complete dissection of all enhancers. *Development* 129, 5667–5681. doi: 10.1242/dev.00157
- Boone, J. Q., and Doe, C. Q. (2008). Identification of *Drosophila* type II neuroblast lineages containing transit amplifying ganglion mother cells. *Dev. Neurobiol.* 68, 1185–1195. doi: 10.1002/dneu.20648
- Bowman, S. K., Rolland, V., Betschinger, J., Kinsey, K. A., Emery, G., and Knoblich, J. A. (2008). The tumor suppressors Brat and Numb regulate transit-amplifying neuroblast lineages in *Drosophila*. *Dev. Cell* 14, 535–546. doi: 10.1016/j.devcel.2008.03.004
- Boyan, G., Liu, Y., Khalsa, S. K., and Hartenstein, V. (2017). A conserved plan for wiring up the fan-shaped body in the grasshopper and *Drosophila*. *Dev. Genes Evol.* 227, 253–269. doi: 10.1007/s00427-017-0587-2
- Chiang, A.-S., Lin, C.-Y., Chuang, C.-C., Chang, H.-M., Hsieh, C.-H., Yeh, C.-W., et al. (2011). Three-dimensional reconstruction of brain-wide wiring networks in *Drosophila* at single-cell resolution. *Curr. Biol.* 21, 1–11. doi: 10.1016/j.cub.2010.11.056
- Costa, M., Manton, J. D., Ostrovsky, A. D., Prohaska, S., and Jefferis, G. S. (2016). NBLAST: rapid, sensitive comparison of neuronal structure and construction of neuron family databases. *Neuron* 91, 293–311. doi: 10.1016/j.neuron.2016.06.012
- Doe, C. Q. (2017). Temporal patterning in the *Drosophila* CNS. *Annu. Rev. Cell Dev. Biol.* 33, 219–240. doi: 10.1146/annurev-cellbio-111315-125210
- Donlea, J. M., Pimentel, D., Talbot, C. B., Kempf, A., Omoto, J. J., Hartenstein, V., et al. (2018). recurrent circuitry for balancing sleep need and sleep. *Neuron* 97, 378.e4–389.e4. doi: 10.1016/j.neuron.2017.12.016
- Dus, M., Ai, M., and Suh, G. S. B. (2013). Taste-independent nutrient selection is mediated by a brain-specific Na<sup>+</sup>/solute co-transporter in *Drosophila*. *Nat. Neurosci.* 16, 526–528. doi: 10.1038/nn.3372
- el Jundi, B., Pfeiffer, K., Heinze, S., and Homberg, U. (2014). Integration of polarization and chromatic cues in the insect sky compass. *J. Comp. Physiol. A Neuroethol. Sens. Neural. Behav. Physiol.* 200, 575–589. doi: 10.1007/s00359-014-0890-6
- el Jundi, B., Warrant, E. J., Byrne, M. J., Khaldy, L., Baird, E., Smolka, J., et al. (2015). Neural coding underlying the cue preference for celestial orientation. *Proc. Natl. Acad. Sci. U.S.A.* 112, 11395–11400. doi: 10.1073/pnas.1501272112
- lab of Gilad Barnea for *trans*-Tango flies (Talay et al., 2017), Mark Frye for TPH-Gal4 (Park et al., 2006), Heinrich Reichert for Poxn-Gal4 (Boll and Noll, 2002), and Barry Dickson for Vienna Tiles driver lines (Tirian and Dickson, 2017). Images from FlyCircuit were obtained from the NCHC (National Center for High-performance Computing) and NTHU (National Tsing Hua University), Hsinchu, Taiwan.
- Franconville, R., Beron, C., and Jayaraman, V. (2018). Building a functional connectome of the *Drosophila* central complex. *eLife* 7:e37017. doi: 10.7444/eLife.37017
- Friggi-Grelin, F., Coulom, H., Meller, M., Gomez, D., Hirsh, J., and Birman, S. (2003). Targeted gene expression in *Drosophila* dopaminergic cells using regulatory sequences from tyrosine hydroxylase. *J. Neurobiol.* 54, 618–627. doi: 10.1002/neu.10185
- Grerer, J. P., Venken, K. J. T., and Dierick, H. A. (2015). Gene-specific cell labeling using MiMIC transposons. *Nucleic Acids Res.* 43:e56. doi: 10.1093/nar/gkv113
- Green, J., Adachi, A., Shah, K. K., Hirokawa, J. D., Magani, P. S., and Maimon, G. (2017). A neural circuit architecture for angular integration in *Drosophila*. *Nature* 546, 101–106. doi: 10.1038/nature22343
- Guo, P., and Ritzmann, R. E. (2013). Neural activity in the central complex of the cockroach brain is linked to turning behaviors. *J. Exp. Biol.* 216, 992–1002. doi: 10.1242/jeb.080473
- Hanesch, U., Fischbach, K. F., and Heisenberg, M. (1989). Neuronal architecture of the central complex in *Drosophila-Melanogaster*. *Cell Tissue Res.* 257, 343–366. doi: 10.1007/BF00261838
- Hartenstein, V., Cruz, L., Lovick, J. K., and Guo, M. (2017). Developmental analysis of the dopamine-containing neurons of the *Drosophila* brain. *J. Comp. Neurol.* 525, 363–379. doi: 10.1002/cne.24069
- Heinze, S. (2017). Unraveling the neural basis of insect navigation. *Curr. Opin. Insect. Sci.* 24, 58–67. doi: 10.1016/j.cois.2017.09.001
- Heinze, S., and Homberg, U. (2007). Maplike representation of celestial E-vector orientations in the brain of an insect. *Science* 315, 995–997. doi: 10.1126/science.1135531
- Heinze, S., and Reppert, S. M. (2011). Sun compass integration of skylight cues in migratory monarch butterflies. *Neuron* 69, 345–358. doi: 10.1016/j.neuron.2010.12.025
- Heinze, S., and Reppert, S. M. (2012). Anatomical basis of sun compass navigation I: the general layout of the monarch butterfly brain. *J. Comp. Neurol.* 520, 1599–1628. doi: 10.1002/cne.23054
- Immonen, E.-V., Dacke, M., Heinze, S., and El Jundi, B. (2017). Anatomical organization of the brain of a diurnal and a nocturnal dung beetle. *J. Comp. Neurol.* 525, 1879–1908. doi: 10.1002/cne.24169
- Ito, K., and Awasaki, T. (2008). “Clonal unit architecture of the adult fly brain,” in *Brain Development in Drosophila melanogaster Advances in Experimental Medicine and Biology*, (New York, NY: Springer), 137–158. doi: 10.1007/978-0-387-78261-4-9
- Ito, K., Shinomiya, K., Ito, M., Armstrong, J. D., Boyan, G., Hartenstein, V., et al. (2014). A systematic nomenclature for the insect brain. *Neuron* 81, 755–765. doi: 10.1016/j.neuron.2013.12.017
- Ito, M., Masuda, N., Shinomiya, K., Endo, K., and Ito, K. (2013). Systematic analysis of neural projections reveals clonal composition of the *Drosophila* brain. *Curr. Biol.* 23, 644–655. doi: 10.1016/j.cub.2013.03.015

## SUPPLEMENTARY MATERIAL

The Supplementary Material for this article can be found online at: <https://www.frontiersin.org/articles/10.3389/fncir.2018.00103/full#supplementary-material>

- Jenett, A., Rubin, G. M., Ngo, T.-T. B., Shepherd, D., Murphy, C., Dionne, H., et al. (2012). A GAL4-driver line resource for *Drosophila* neurobiology. *Cell Rep.* 2, 991–1001. doi: 10.1016/j.celrep.2012.09.011
- Kumar, A., Bello, B., and Reichert, H. (2009). Lineage-specific cell death in postembryonic brain development of *Drosophila*. *Development* 136, 3433–3442. doi: 10.1242/dev.037226
- Kuntz, S., Poeck, B., Sokolowski, M. B., and Strauss, R. (2012). The visual orientation memory of *Drosophila* requires foraging (PKG) upstream of ignorant (RSK2) in ring neurons of the central complex. *Learn. Mem.* 19, 337–340. doi: 10.1101/lm.026369.112
- Larsen, C., Shy, D., Spindler, S. R., Fung, S., Peraanu, W., Younossi-Hartenstein, A., et al. (2009). Patterns of growth, axonal extension and axonal arborization of neuronal lineages in the developing *Drosophila* brain. *Dev. Biol.* 335, 289–304. doi: 10.1016/j.ydbio.2009.06.015
- Lee, T., and Luo, L. (1999). Mosaic analysis with a repressible cell marker for studies of gene function in neuronal morphogenesis. *Neuron* 22, 451–461. doi: 10.1016/S0896-6273(00)80701-1
- Lin, C.-Y., Chuang, C.-C., Hua, T.-E., Chen, C.-C., Dickson, B. J., Greenspan, R. J., et al. (2013). A comprehensive wiring diagram of the protocerebral bridge for visual information processing in the *Drosophila* brain. *Cell Rep.* 3, 1739–1753. doi: 10.1016/j.celrep.2013.04.022
- Liu, Q., Tabuchi, M., Liu, S., Kodama, L., Horiuchi, W., Daniels, J., et al. (2017). Branch-specific plasticity of a bifunctional dopamine circuit encodes protein hunger. *Science* 356, 534–539. doi: 10.1126/science.aal3245
- Liu, S., Liu, Q., Tabuchi, M., and Wu, M. N. (2016). Sleep drive is encoded by neural plastic changes in a dedicated circuit. *Cell* 165, 1347–1360. doi: 10.1016/j.cell.2016.04.013
- Lovick, J. K., and Hartenstein, V. (2015). Hydroxyurea-mediated neuroblast ablation establishes birth dates of secondary lineages and addresses neuronal interactions in the developing *Drosophila* brain. *Dev. Biol.* 402, 32–47. doi: 10.1016/j.ydbio.2015.03.005
- Lovick, J. K., Ngo, K. T., Omoto, J. J., Wong, D. C., Nguyen, J. D., and Hartenstein, V. (2013). Postembryonic lineages of the *Drosophila* brain: I. Development of the lineage-associated fiber tracts. *Dev. Biol.* 384, 228–257. doi: 10.1016/j.ydbio.2013.07.008
- Lovick, J. K., Omoto, J. J., Ngo, K. T., and Hartenstein, V. (2017). Development of the anterior visual input pathway to the *Drosophila* central complex. *J. Comp. Neurol.* 525, 3458–3475. doi: 10.1002/cne.24277
- Martin, J. P., Guo, P., Mu, L., Harley, C. M., and Ritzmann, R. E. (2015). Central-complex control of movement in the freely walking cockroach. *Curr. Biol.* 25, 2795–2803. doi: 10.1016/j.cub.2015.09.044
- Martin, J. R., Raabe, T., and Heisenberg, M. (1999). Central complex substructures are required for the maintenance of locomotor activity in *Drosophila melanogaster*. *J. Comp. Physiol. A* 185, 277–288. doi: 10.1007/s003590050387
- Martín-Peña, A., Acebes, A., Rodríguez, J. R., Chevalier, V., Casas-Tinto, S., Triphan, T., et al. (2014). Cell types and coincident synapses in the ellipsoid body of *Drosophila*. *Eur. J. Neurosci.* 39, 1586–1601. doi: 10.1111/ejn.12537
- Minocha, S., Boll, W., and Noll, M. (2017). Crucial roles of pox neuro in the developing ellipsoid body and antennal lobes of the *Drosophila* brain. *PLoS One* 12:e0176002. doi: 10.1371/journal.pone.0176002
- Müller, M., Homberg, U., and Kühn, A. (1997). Neuroarchitecture of the lower division of the central body in the brain of the locust (*Schistocerca gregaria*). *Cell Tissue Res.* 288, 159–176. doi: 10.1007/s004410050803
- Namiki, S., and Kanzaki, R. (2016). Comparative neuroanatomy of the lateral accessory lobe in the insect brain. *Front. Physiol.* 7:244. doi: 10.3389/fphys.2016.00244
- Nern, A., Pfeiffer, B. D., and Rubin, G. M. (2015). Optimized tools for multicolor stochastic labeling reveal diverse stereotyped cell arrangements in the fly visual system. *Proc. Natl. Acad. Sci. U.S.A.* 112, E2967–E2976. doi: 10.1073/pnas.1506763112
- Neuser, K., Triphan, T., Mronz, M., Poeck, B., and Strauss, R. (2008). Analysis of a spatial orientation memory in *Drosophila*. *Nature* 453, 1244–1247. doi: 10.1038/nature07003
- Nicolaï, L. J. J., Ramaekers, A., Raemaekers, T., Drozdzecki, A., Mauss, A. S., Yan, J., et al. (2010). Genetically encoded dendritic marker sheds light on neuronal connectivity in *Drosophila*. *Proc. Natl. Acad. Sci. U.S.A.* 107, 20553–20558. doi: 10.1073/pnas.1010198107
- Ofstad, T. A., Zuker, C. S., and Reiser, M. B. (2011). Visual place learning in *Drosophila melanogaster*. *Nature* 474, 204–207. doi: 10.1038/nature10131
- Omoto, J. J., Keleş, M. F., Nguyen, B.-C. M., Bolanos, C., Lovick, J. K., Frye, M. A., et al. (2017). Visual input to the *Drosophila* central complex by developmentally and functionally distinct neuronal populations. *Curr. Biol.* 27, 1098–1110. doi: 10.1016/j.cub.2017.02.063
- Omoto, J. J., Nguyen, B.-C. M., Kandimalla, P., Lovick, J. K., Donlea, J. M., and Hartenstein, V. (2018). Neuronal constituents and putative interactions within the *Drosophila* ellipsoid body neuropil. *bioRxiv* [Preprint]. doi: 10.1101/394833
- Park, J., Lee, S. B., Lee, S., Kim, Y., Song, S., Kim, S., et al. (2006). Mitochondrial dysfunction in *Drosophila* PINK1 mutants is complemented by parkin. *Nature* 441, 1157–1161. doi: 10.1038/nature04788
- Park, J.-Y., Dus, M., Kim, S., Abu, F., Kanai, M. I., Rudy, B., et al. (2016). *Drosophila* SLCSA11 mediates hunger by regulating K(+) channel activity. *Curr. Biol.* 26, 1965–1974. doi: 10.1016/j.cub.2016.05.076
- Peraanu, W., and Hartenstein, V. (2006). Neural lineages of the *Drosophila* brain: a three-dimensional digital atlas of the pattern of lineage location and projection at the late larval stage. *J. Neurosci.* 26, 5534–5553. doi: 10.1523/JNEUROSCI.4708-05.2006
- Peraanu, W., Kumar, A., Jenett, A., Reichert, H., and Hartenstein, V. (2010). Development-based compartmentalization of the *Drosophila* central brain. *J. Comp. Neurol.* 518, 2996–3023. doi: 10.1002/cne.22376
- Pfeiffer, K., and Homberg, U. (2014). Organization and functional roles of the central complex in the insect brain. *Annu. Rev. Entomol.* 59, 165–184. doi: 10.1146/annurev-ento-011613-162031
- Pooryasin, A., and Fiala, A. (2015). Identified serotonin-releasing neurons induce behavioral quiescence and suppress mating in *Drosophila*. *J. Neurosci.* 35, 12792–12812. doi: 10.1523/JNEUROSCI.1638-15.2015
- Ren, Q., Awasaki, T., Huang, Y.-F., Liu, Z., and Lee, T. (2016). Cell class-lineage analysis reveals sexually dimorphic lineage compositions in the *Drosophila* brain. *Curr. Biol.* 26, 2583–2593. doi: 10.1016/j.cub.2016.07.086
- Renn, S. C., Armstrong, J. D., Yang, M., Wang, Z., An, X., Kaiser, K., et al. (1999). Genetic analysis of the *Drosophila* ellipsoid body neuropil: organization and development of the central complex. *J. Neurobiol.* 41, 189–207. doi: 10.1002/(SICI)1097-4695(19991105)41:2<189::AID-NEU3>3.0.CO;2-Q
- Rieche, F., Carmine-Simmen, K., Poeck, B., Kretschmar, D., and Strauss, R. (2018). *Drosophila* full-length amyloid precursor protein is required for visual working memory and prevents age-related memory impairment. *Curr. Biol.* 28, 817.e3–823.e3. doi: 10.1016/j.cub.2018.01.077
- Schindelin, J., Arganda-Carreras, I., Frise, E., Kaynig, V., Longair, M., Pietzsch, T., et al. (2012). Fiji: an open-source platform for biological-image analysis. *Nat. Methods* 9, 676–682. doi: 10.1038/nmeth.2019
- Seelig, J. D., and Jayaraman, V. (2013). Feature detection and orientation tuning in the *Drosophila* central complex. *Nature* 503, 262–266. doi: 10.1038/nature12601
- Seelig, J. D., and Jayaraman, V. (2015). Neural dynamics for landmark orientation and angular path integration. *Nature* 521, 186–191. doi: 10.1038/nature14446
- Shiozaki, H. M., and Kazama, H. (2017). Parallel encoding of recent visual experience and self-motion during navigation in *Drosophila*. *Nat. Neurosci.* 20, 1395–1403. doi: 10.1038/nn.4628
- Spindler, S. R., and Hartenstein, V. (2010). The *Drosophila* neural lineages: a model system to study brain development and circuitry. *Dev. Genes Evol.* 220, 1–10. doi: 10.1007/s00427-010-0323-7
- Spindler, S. R., and Hartenstein, V. (2011). Bazooka mediates secondary axon morphology in *Drosophila* brain lineages. *Neural Dev.* 6:16. doi: 10.1186/1749-8104-6-16
- Strausfeld, N. J. (ed.) (2012). *Atlas of an Insect Brain*. Berlin: Springer Science & Business Media, doi: 10.1007/978-3-642-66179-2
- Strauss, R., and Heisenberg, M. (1993). A higher control center of locomotor behavior in the *Drosophila* brain. *J. Neurosci.* 13, 1852–1861. doi: 10.1523/JNEUROSCI.13-05-01852.1993
- Sun, Y., Nern, A., Franconville, R., Dana, H., Schreiter, E. R., Looger, L. L., et al. (2017). Neural signatures of dynamic stimulus selection in *Drosophila*. *Nat. Neurosci.* 20, 1104–1113. doi: 10.1038/nn.4581
- Talay, M., Richman, E. B., Snell, N. J., Hartmann, G. G., Fisher, J. D., Sorkaç, A., et al. (2017). Transsynaptic mapping of second-order taste neurons in flies by trans-tango. *Neuron* 96, 783.e4–795.e4. doi: 10.1016/j.neuron.2017.10.011

- Thran, J., Poeck, B., and Strauss, R. (2013). Serum response factor-mediated gene regulation in a *Drosophila* visual working memory. *Curr. Biol.* 23, 1756–1763. doi: 10.1016/j.cub.2013.07.034
- Tirian, L., and Dickson, B. (2017). The VT GAL4, LexA, and split-GAL4 driver line collections for targeted expression in the *Drosophila* nervous system. *bioRxiv* [Preprint]. doi: 10.1101/198648
- Turner-Evans, D., Wegener, S., Rouault, H., Franconville, R., Wolff, T., Seelig, J. D., et al. (2017). Angular velocity integration in a fly heading circuit. *eLife* 6:e04577. doi: 10.7554/eLife.23496
- Varga, A. G., and Ritzmann, R. E. (2016). Cellular basis of head direction and contextual cues in the insect brain. *Curr. Biol.* 26, 1816–1828. doi: 10.1016/j.cub.2016.05.037
- von Hadeln, J., Althaus, V., Häger, L., and Homberg, U. (2018). Anatomical organization of the cerebrum of the desert locust *Schistocerca gregaria*. *Cell Tissue Res.* 178, 199–224. doi: 10.1007/s00441-018-2844-8
- Wang, Y.-C., Yang, J. S., Johnston, R., Ren, Q., Lee, Y.-J., Luan, H., et al. (2014). *Drosophila* intermediate neural progenitors produce lineage-dependent related series of diverse neurons. *Development* 141, 253–258. doi: 10.1242/dev.103069
- Wolff, T., Iyer, N. A., and Rubin, G. M. (2015). Neuroarchitecture and neuroanatomy of the *Drosophila* central complex: a GAL4-based dissection of protocerebral bridge neurons and circuits. *J. Comp. Neurol.* 523, 997–1037. doi: 10.1002/cne.23705
- Wolff, T., and Rubin, G. M. (2018). Neuroarchitecture of the *Drosophila* central complex: a catalog of nodulus and asymmetrical body neurons and a revision of the protocerebral bridge catalog. *J. Comp. Neurol.* doi: 10.1002/cne.24512 [Epub ahead of print].
- Wong, D. C., Lovick, J. K., Ngo, K. T., Borisuthirattana, W., Omoto, J. J., and Hartenstein, V. (2013). Postembryonic lineages of the *Drosophila* brain: II. Identification of lineage projection patterns based on MARCM clones. *Dev. Biol.* 384, 258–289. doi: 10.1016/j.ydbio.2013.07.009
- Xie, X., Tabuchi, M., Brown, M. P., Mitchell, S. P., Wu, M. N., and Kolodkin, A. L. (2017). The laminar organization of the *Drosophila* ellipsoid body is semaphorin-dependent and prevents the formation of ectopic synaptic connections. *eLife* 6:e04577. doi: 10.7554/eLife.25328
- Yang, J. S., Awasaki, T., Yu, H.-H., He, Y., Ding, P., Kao, J.-C., et al. (2013). Diverse neuronal lineages make stereotyped contributions to the *Drosophila* locomotor control center, the central complex. *J. Comp. Neurol.* 521, 2645–2662. doi: 10.1002/cne.23339
- Young, J. M., and Armstrong, J. D. (2010a). Building the central complex in *Drosophila*: the generation and development of distinct neural subsets. *J. Comp. Neurol.* 518, 1525–1541. doi: 10.1002/cne.22285
- Young, J. M., and Armstrong, J. D. (2010b). Structure of the adult central complex in *Drosophila*: organization of distinct neuronal subsets. *J. Comp. Neurol.* 518, 1500–1524. doi: 10.1002/cne.22284
- Yu, H.-H., Awasaki, T., Schroeder, M. D., Long, F., Yang, J. S., He, Y., et al. (2013). Clonal development and organization of the adult *Drosophila* central brain. *Curr. Biol.* 23, 633–643. doi: 10.1016/j.cub.2013.02.057
- Zhao, X., Lenek, D., Dag, U., Dickson, B. J., and Keleman, K. (2018). Persistent activity in a recurrent circuit underlies courtship memory in *Drosophila*. *eLife* 7:e04577. doi: 10.7554/eLife.31425
- Zheng, Z., Lauritzen, J. S., Perlman, E., Robinson, C. G., Nichols, M., Milkie, D., et al. (2018). A complete electron microscopy volume of the brain of adult *Drosophila melanogaster*. *Cell* 174, 730.e22–743.e22. doi: 10.1016/j.cell.2018.06.019

**Conflict of Interest Statement:** The authors declare that the research was conducted in the absence of any commercial or financial relationships that could be construed as a potential conflict of interest.

Copyright © 2018 Omoto, Nguyen, Kandimalla, Lovick, Donlea and Hartenstein. This is an open-access article distributed under the terms of the Creative Commons Attribution License (CC BY). The use, distribution or reproduction in other forums is permitted, provided the original author(s) and the copyright owner(s) are credited and that the original publication in this journal is cited, in accordance with accepted academic practice. No use, distribution or reproduction is permitted which does not comply with these terms.